THERMAL EXPANSION BEHAVIOUR OF SOME OXIDE SPINELS

AKRAM ATTA AL-AJAJ

A thesis submitted for the degree of

Doctor of Philosophy

The University of Aston in Birmingham

August - 1984

The University of Aston in Birmingham

AKRAM ATTA AL-AJAJ, B.Sc., M.Sc.

Thermal Expansion Behaviour of Some Oxide Spinels

A thesis submitted for the degree of Doctor of Philosophy

1984

SUMMARY

Compounds which crystallize with the cubic spinel structure are believed to be unusually anharmonic.

This work is concerned with investigating the anharmonicity in $MgAl_2O_4$ and $ZnFe_2O_4$ spinels. The experimental method depends on exploiting Grüneisen's law which states that in the case of a harmonic solid, the coefficient of thermal expansion is proportional to the heat capacity at that temperature.

The heat capacity data of $MgAl_2O_4$ and $ZnFe_2O_4$ spinels are known over the low temperature range between 77.5 K and room temperature. Therefore if the thermal expansion is measured over the same temperature range, the validity of Grüneisen's law can be tested, and some measure of anharmonicity can be derived from any discrepancies.

A combination of X-ray equipment with low temperature attachments has been used to measure the lattice constants of the two spinels over a range of temperature 77.5 - 300.1 K°. This experimental data, corrected by means of an internal standard, was smoothed by curve fitting, to provide results for the coefficient of thermal expansion for the two compounds over a corresponding range of temperature.

Finally, these new results are compared with the thermal expansion and Grüneisen parameter behaviour of silicon and related materials and with the behaviour of other spinels where data are already available.

Key words:
Spinel
Anharmonicity
Thermal expansion
Grüneisen's law

CONTENTS

LIST OF TABLES

LIST OF FIGURES

LIST OF SYMBOLS

P^{2+}	Divalent cation
Q^{3+}	Trivalent cation
X^{2-}	Divalent anion
U	Anion position parameter
hko	Miller indices with $\ell = 0$
ϕ	Potential energy
r	Nearest neighbour separation
α, β	Linear and volume coefficients of thermal expansion respectively
V	Molar volume
χ_T, χ_S	Isothermal and adiabatic compressibility respectively
C_p, C_v	Molar heat capacity at constant pressure and volume respectively
γ	Grüneisen parameter
θ	Bragg angle
θ_c	Centroid Bragg angle
$\Delta\theta$	Line position correction
d	Interplanar distance
λ	Wavelength
λ_c	Centroid wavelength
a	Lattice parameter
θ_o	Debye temperature

CHAPTER 1

SPINEL AN ANHARMONIC MATERIAL?

1.1 Introduction

There are a great many compounds which crystallize with the same crystal structure as the mineral known as spinel. Many of these compounds, though not all, have the general formula $P^{2+}Q_2^{3+}X_4^{2-}$, where P^{2+} and Q^{3+} may be replaced by a wide range of divalent and trivalent cations respectively. Similarly, replacement of X^{2-} leads to series classified as oxide, sulphide, selenide and telluride spinels.

The structure is unusual in that if X is a divalent anion, P and Q may also take valences of 2 and 4 or even 1 and 6, and it is easily seen that, when this flexibility is added to that already mentioned, the number of possible chemical combinations must be very extensive indeed. It is therefore scarcely surprising to find that more than 200 compounds can be said to belong to the spinel series. This enormous chemical versatility is reflected in the wide variation of physical behaviour which can occur among the spinel compounds. For example, oxides are usually insulators (when stoichiometric) while sulphides and

selenides may be semiconductors or metallic. Similarly, magnetic behaviour depends upon the absence or presence of transition elements. The practical importance of the spinel ferrites MFe_2O_4, where M may be Cu, Ni, or Co, then arises from the property of being simultaneously both ferrimagnetic and electrically insulating. Such materials are widely exploited in the modern telecommunications industry. Other materials used in this way include magnetite which can form the coating for magnetic recording tapes and single crystal magnesium aluminate used as substrate material for the epitaxial growth of thin films of silicon and related semiconductors (Manasevit and Forbes, 1966; Wang et al, 1974; Ladany and Wang, 1974).

The spinels are, therefore, of considerable interest from a technical point of view. A general review of the industrial applications of the spinel groups of compounds has been given by Grimes (1975).

1.2 The spinel structure

A crystal structure for spinel was first proposed by Bragg (1915) and at the same time by Nishikawa (1915). They showed by X-ray diffraction that spinel is cubic and that the unit cell must contain eight formula units.

The essential features of this unit cell are shown in

Figure 1.1. The oxygen ions, which are physically the largest, form a nearly close-packed cubic array within which the metal ions occupy certain interstitial positions. Two types of these interstices are important, 64 having fourfold coordination, of which 8, the A-sites, may be occupied by divalent cations, and 32 having sixfold coordination, of which 16, the B-sites, may be occupied by the trivalent cations. The site symmetries and overall symmetry are then usually assumed to conform with the crystallographic space group Fd3m for which some details are given in Table 1.1.

This table shows that when the conventional space group is chosen the cations are in special positions uniquely determined by symmetry, and the structure is centro-symmetrical about the B-site. In addition, the anion positions are completely specified in terms of a single positional parameter u, which, for an ideal spinel with perfect anion packing, has a value of 3/8. In practice, u is often found to be larger, and for u > 3/8 the anions move in < 111 > directions outwards from the nearest A-site. These displacements destroy the perfect octahedral geometry which would exist around the B-sites in perfect packing and result in a local distortion at those positions of symmetry $\bar{3}$m.

Two features have been neglected in this description. Firstly, an ideal cation distribution over the A- and B-

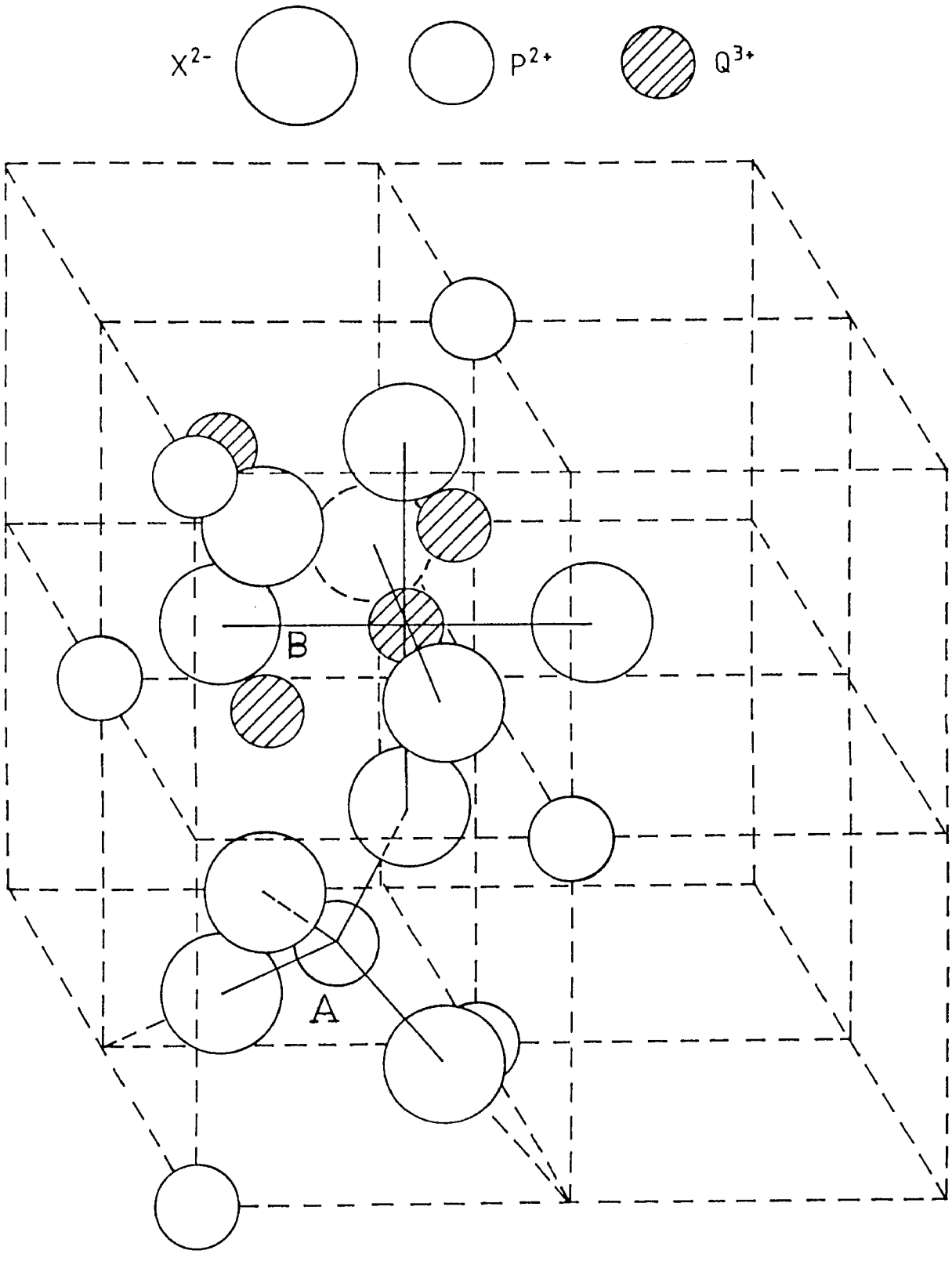

Figure 1.1 Spinel structure (Gorter, 1954)

Atom position	No of positions	Local Symmetry	Position Co-ordinates
A - site	8	$\bar{4}3m$	F.C.C. translations + 000; $\frac{1}{4}$, $\frac{1}{4}$, $\frac{1}{4}$;
B - site	16	$\bar{3}m$	$\frac{5}{8}$ $\frac{5}{8}$ $\frac{5}{8}$; $\frac{7}{8}$ $\frac{7}{8}$ $\frac{5}{8}$; $\frac{7}{8}$ $\frac{5}{8}$ $\frac{7}{8}$; $\frac{5}{8}$ $\frac{7}{8}$ $\frac{7}{8}$;
Anion position	32	3m	UUU, $\frac{1}{4}$ - U, $\frac{1}{4}$ - U, $\frac{1}{4}$ - U; $\bar{U}\bar{U}U$, $\frac{1}{4}$ + U, $\frac{1}{4}$ + U, $\frac{1}{4}$ - U; $\bar{U}U\bar{U}$, $\frac{1}{4}$ + U, $\frac{1}{4}$ - U, $\frac{1}{4}$ + U; $U\bar{U}\bar{U}$, $\frac{1}{4}$ - U, $\frac{1}{4}$ + U, $\frac{1}{4}$ + U;

Table 1.1

Atom positions according to space group Fd3m

sites has been assumed, a limiting case commonly described as the 'normal' structure. An alternative limiting case, the 'inverse' structure has A-sites occupied by half the trivalent cations while B-sites are randomly shared between the remaining trivalent cations and the divalent cations. Experimental studies of diffraction patterns have shown that many spinels have intermediate cation arrangements so that a more general representation of the spinel structure would be

$$P_x^{2+}\ Q_{1-x}^{3+}\ [P_{1-x}^{2+}\ Q_{1+x}^{3+}]\ O_4$$

where x is a measure of the degree of inversion.

Finally, it should be emphasized that the conventional choice of space group is very restrictive for possible atom positions and therefore, for the physical behaviour of the spinel groups of materials, as will be explained later, there is much good experimental evidence now favouring the choice of a non-centrosymmetrical space group $F\bar{4}3m$. This alternative symmetry allows the anion positions to be divided into two groups with different position parameters together with some flexibility for the position of the cations in B-sites as shown in Table 1.2 and Figure 1.2.

Atom position	No of positions	Local Symmetry	Position Co-ordinates
A_1- site	4	$\bar{4}3m$	F.C.C. translations + 0,0,0;
A_2-site	4	$\bar{4}3m$	$\frac{1}{4}, \frac{1}{4}, \frac{1}{4}$;
B - site	16	3m	X_1, X_1, X_1; $\bar{X}_1, \bar{X}_1, X_1$; $\bar{X}_1, X_1, \bar{X}_1$; $X_1, \bar{X}_1, \bar{X}_1$;
Anion position 1	16	3m	X_2, X_2, X_2; $\bar{X}_2, \bar{X}_2, X_2$; $\bar{X}_2, X_2, \bar{X}_2$; $X_2, \bar{X}_2, \bar{X}_2$
Anion position 2	16	3m	X_3, X_3, X_3; $\bar{X}_3, \bar{X}_3, X_3$; $\bar{X}_3, X_3, \bar{X}_3$; $X_3, \bar{X}_3, \bar{X}_3$;

Table 1.2

Atom positions according to space group $F\bar{4}3m$

X_1 , X_2 and X_3 parameters describe atom shifts from the perfect configuration.

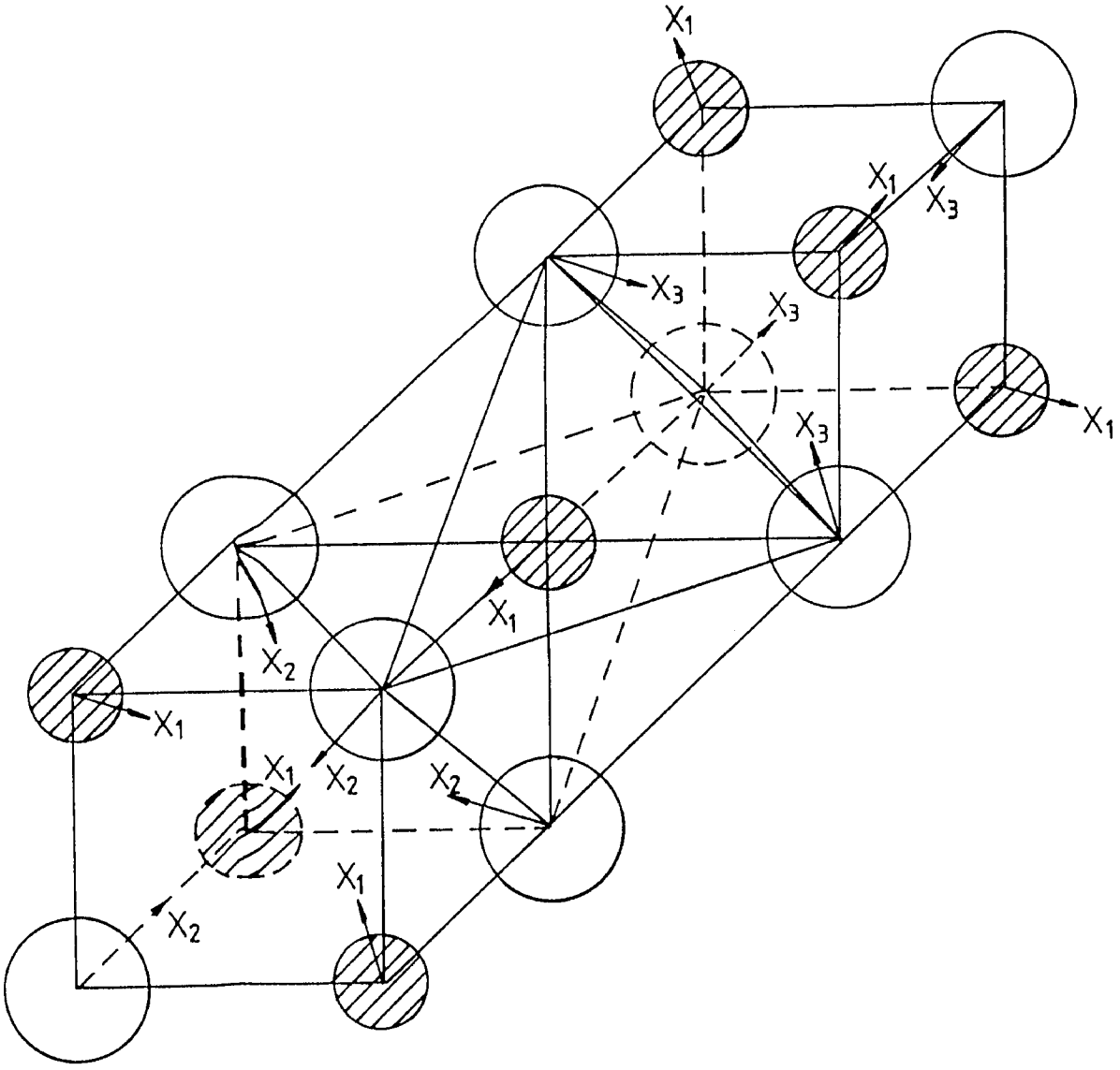

Figure 1.2 Octahedral site under $F\bar{4}3m$ symmetry

1.3 Physical evidence in favour of $F\bar{4}3m$ symmetry

1.3.1 Indirect evidence

Crystallographic phase transitions are extremely common among the spinel compounds, the transformation usually involving a change from cubic to tetragonal symmetry with decreasing temperature. According to Dunitz and Orgel (1957) this may be understood as a manifestation of the Jahn-Teller effect, as the compounds concerned invariably contain transition ions like Cu^{2+}, Fe^{2+} or Mn^{3+} in which the electronic ground states are orbitally degenerate. In such spinels, it is believed that local structure distortions develop above the transition temperature in the cubic phase and that these increase in orientational coherence as the temperature decreases until their influence is eventually sufficient to induce an overall structural change (see for example Finch et al, 1958), the physical evidence supporting this description of the cubic phase includes the observation of Debye-Waller factor enhancement in X-ray diffraction (Cervinka, 1965), Mössbauer spectra (Tanaka et al, 1966) and complexities in the infra-red absorption spectra (Brabers, 1969). The latter are particularly significant as the additional absorption bands can be shown to correspond with those from a tetragonal spinel (e.g. Mn_3O_4) by examination of the spectra across a compositional range like $Mn_xFe_{3-x}O_4$.

In contrast to compounds of this kind, a cubic spinel series such as $Mg[Cr_xAl_{2-x}]O_4$ would be expected to be physically well behaved. The Cr^{3+} ion has the most marked octahedral site preference of any in the first transition series (McClure, 1957) and an electronic ground state in octahedral surroundings with no orbital degeneracy when Hund's rules are obeyed, i.e. no Jahn-Teller effect is expected. Nevertheless, X-ray diffraction studies by Grimes and Hilleard (1970) showed that increasing x in this series was accompanied by a substantial increase in Debye-Waller factor in exactly analogous manner to the earlier observations of Cervinka on the Jahn-Teller series $Mn_xFe_{3-x}O_4$. The conclusion was drawn that structural distortions must also exist in the chromite series and moreover, that they must increase in severity with increase in chromium content.

Very similar conclusions were reached by Lou and Ballentyne (1968) from a study of the optical fluorescent spectra from a series of synthetic single crystals of the $Mg[Cr_xAl_{2-x}]O_4$ spinel group, an important feature of these spectra being, that above a chromium concentration of 2wt% a new selection rule is observed which identifies the symmetry of the octahedral site occupied by Cr^{3+} ions as 3m (see Figure 1.3). The significance of the latter lies in the fact that it is incompatible with the crystallographic spinel group to which the spinel structure is normally referred but consistent with the X-ray

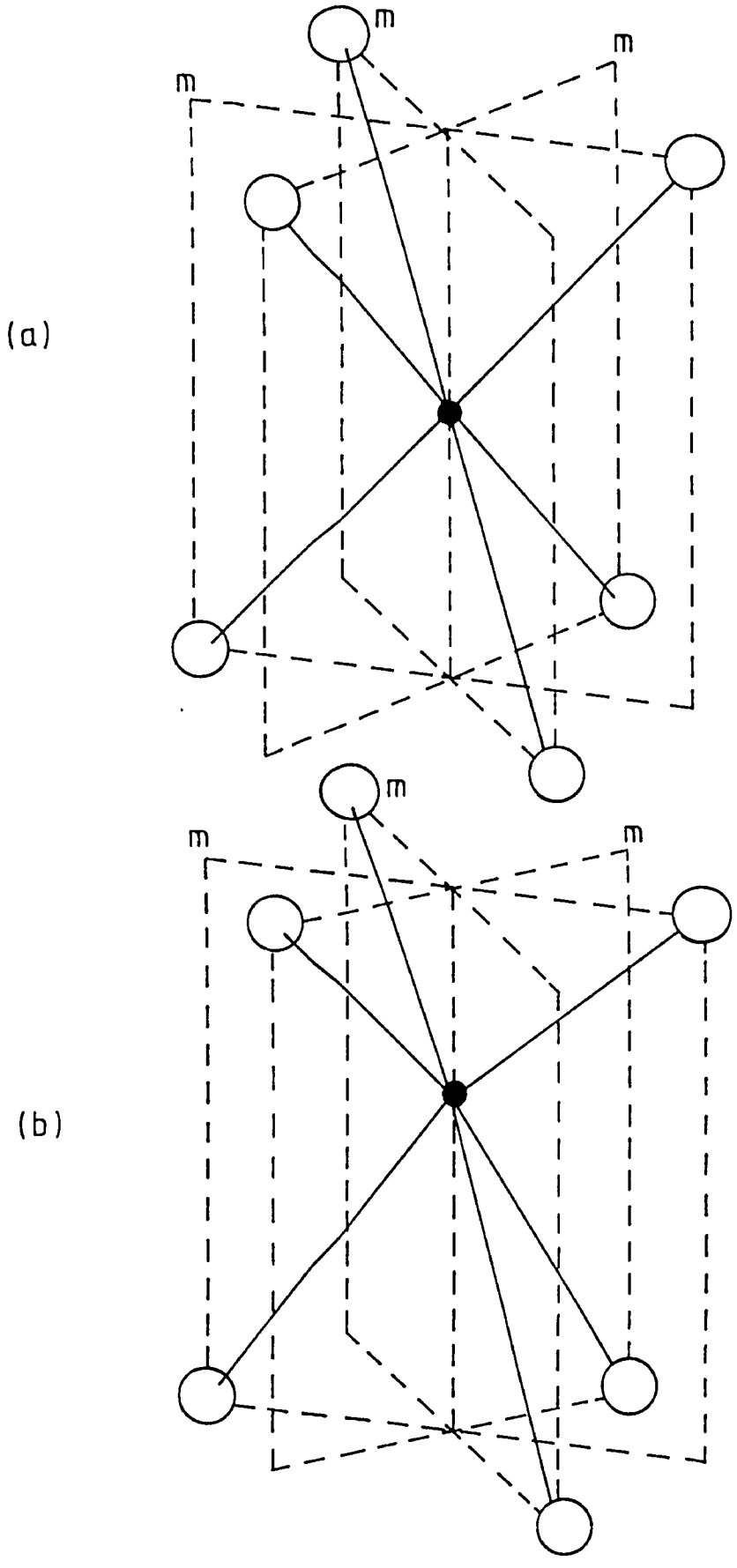

Figure 1.3 Illustration of the difference between (a) $\bar{3}$m and (b) 3m site symmetries.

diffraction observations, for if the local trigonal distortions had been of conventional $\bar{3}$m symmetry an increase in severity would have been brought about through an increase in the oxygen position parameter u. According to Grimes and Hilleard, however, no change in this parameter was detectable within experimental error.

In experiments such as these in which magnesium aluminate is lightly doped with chromium, the local structural distortions might be expected to be displaced among the octahedral sites according to the distribution of the Cr^{3+} ions, but it is possible, however, to envisage local 3m distortions which are organised in a regular periodic manner throughout the whole crystal (see Figure 1.4). In the latter case, it is difficult to escape the conclusion that the distortion of the octahedral sites is something inherent in the spinel structure which corresponds to a change of space group symmetry to F$\bar{4}$3m.

According to this view a change in physical behaviour through a spinel series can be understood as arising from a change in the degree of structural asymmetry rather than as a change in the proportion of distorted to undistorted material and thus the change of space group was used by Grimes and Collett (1971) to account for changes in the complexity of the infra-red absorption spectrum through the series $Mg[Cr_xAl_{2-x}]O_4$. Their observations, similar to those of Brabers (1969) on the Jahn-Teller series

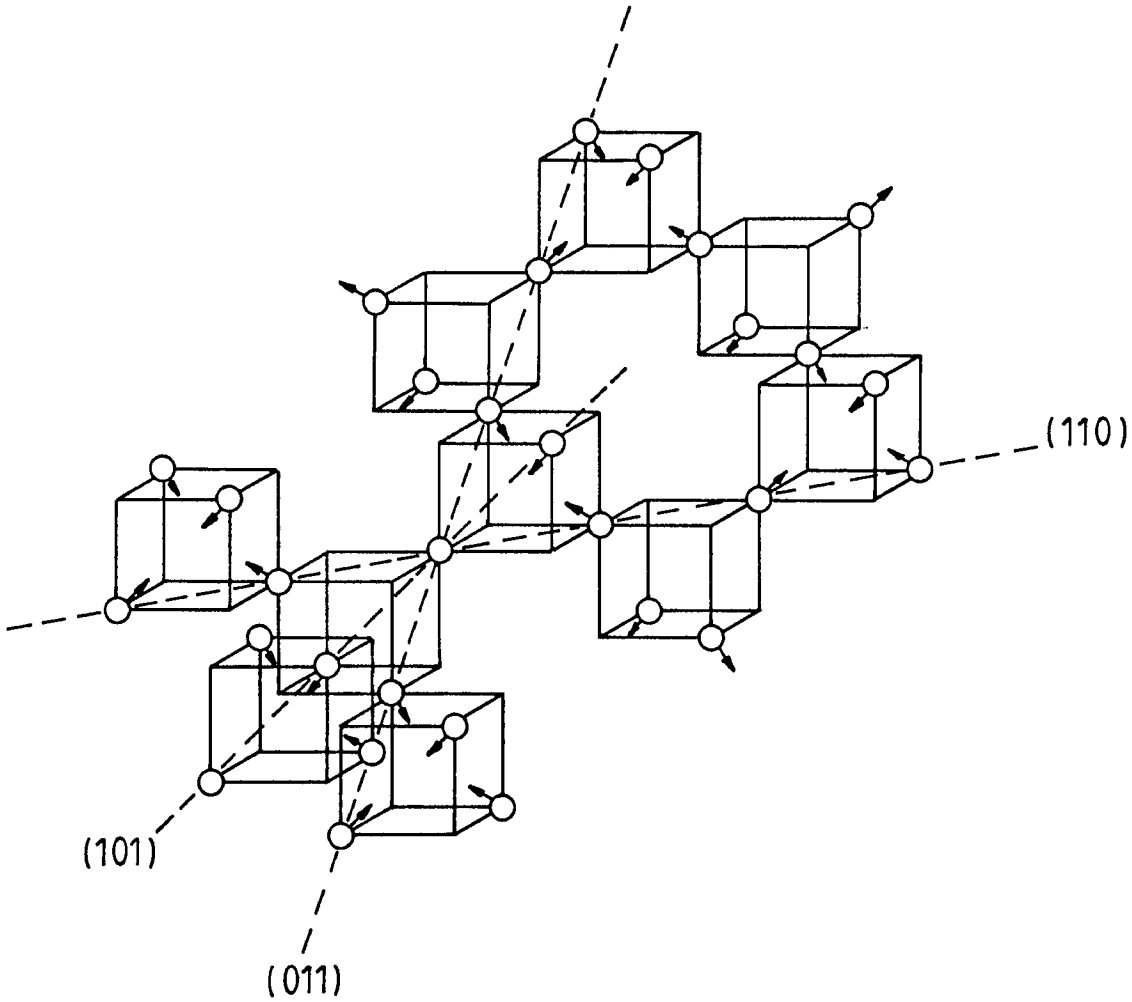

Figure 1.4 Octahedral ion sublattice.

$Mn_xFe_{3-x}O_4$, were made on some polycrystalline samples previously investigated by X-ray diffraction (Grimes and Hilleard, 1970) and showed an increase in the number of absorption peaks from four in $MgAl_2O_4$ up to seven in $MgCr_2O_4$.

Now the possibility that the chromites are alone among the closely related spinel compounds in possessing a crystal structure of $F\bar{4}3m$ symmetry must be considered to be very unlikely and it was therefore suggested by Grimes (1971, 1972a) that the spinel structure might more generally be referred to $F\bar{4}3m$. It had been known for many years, for example, that some of the spinel ferrites have dielectric constants which can rise by several orders of magnitude, typically 10^2 to 10^4, at low frequencies (see for instance the observations of Polder (1950) on certain Mn-Zn and Ni-Zn ferrites) and it would seem natural to explain these observations in terms of permanent dipoles similar to those found in $BaTiO_3$. However, as Fairweather et al (1952) realised, ferroelectricity is excluded by the centro-symmetric space group Fd3m to which the crystal structure had conventionally been referred and consequently the interpretation of low-frequency dielectric behaviour has presented considerable theoretical difficulties. In some cases, because measurements were made on polycrystalline specimens, it has been possible to explain the experimental observations in terms of a phenomenological model (Koops, 1951) where the dielectric is considered to be

composed of good conducting crystallites separated by poor conducting intersurface layers. On the other hand, the resistivity and dielectric behaviour reported by Van Uitert (1956) for certain Ni-Mn ferrites and by Peters and Standley (1958) for Mg-Mn ferrite appear to be quite different. The latter authors in particular were clearly seeking a crystallographic explanation as they state that (for $Mg_{0.1}Mn_{0.9}Fe_2O_4$) ..... "The temperature and frequency dependence of the dielectric constant is very similar to that found when true dielectric relaxation is occurring and, an explanation of the results ..... in terms of the relaxation of permanent dipoles within the ferrite is envisaged. An order of magnitude calculation suggests that the high dielectric constant at low frequencies found at 200°C may be explained by the presence of permanent dipole moments of the order of 0.5 debye, indicating an effective charge separation of the order of 0.1 Å".

These observations are clearly of considerable importance in the context of the proposed change of space group for spinel, for the order of magnitude of the ionic displacements envisaged by Grimes as responsible for the change of symmetry, accounts precisely for the magnitude of the dipole moment estimated by Peters and Standley. Moreover, as emphasized by Grimes (1973a), the symmetry of ionic movements in $F\bar{4}3m$, shown in Figure 1.4, is consistent with the absence of ferroelectricity noted by

Fairweather et al for the dipole moments which are created are arranged in opposite senses so that the property should be anti-ferroelectricity.

1.3.2 Direct evidence

It is easy in principle to distinguish between the two space groups by diffraction since hko reflexions with $h + k = 4n + 2$ are forbidden by Fd3m but allowed by $F\bar{4}3m$. When the deviations from conventional symmetry are small, however, the Fd3m forbidden reflexions can be very weak and difficult to confirm. Thus the first reported observations of such forbidden reflexions in electron diffraction from $MgAl_2O_4$ (the x = 0 end number of the $Mg[Cr_xAl_{2-x}]O_4$ series) by Hwang et al (1973), (see also Heuer and Mitchell, 1975), were greeted with considerable scepticism. For example, Samuelsen and Steinsvoll (1975) have searched without success for a 200 reflexion from $MgAl_2O_4$ using a neutron time-of-flight technique and conclude that 'to a very high accuracy such reflexions are absent', while Smith (1978) attributes the earlier electron diffraction observations to double diffraction involving high-order reflexions in the first-order Laue zone (even though Heuer and Mitchell explain that care was taken to exclude this possibility).

Further direct evidence for $F\bar{4}3m$ symmetry is provided by a

structure analysis of the normal 2-4 spinel γ-Ni_2SiO_4 where the presence of a residual electron density in the final Fourier difference synthesis was revealed (Marumo et al, 1974). In this case, intensities were collected using MoKα X-radiation and 212 independent relfexions were used in a least squares refinement based on the space group Fd3m to achieve an overall residual index R = 1.7% with individual anisotropic temperature factors. The final Fourier difference synthesis showed eight quite prominent peaks 0.46 A^O from the Ni ion in the 8 <111> directions. The height of these peaks was on average about $2eA^{O-3}$ and the authors attributed their existence to a charge density asymmetry around the Ni^{2+} ion. However, a simpler interpretation based on the space group $F\bar{4}3m$ now seems more likely.

The most complete evidence is provided by the recent single crystal diffraction study of $MgAl_2O_4$ in which refinements of atom position and thermal parameters under Fd3m and $F\bar{4}3m$ symmetry were compared, using a substantial range of intensity data (Grimes et al, 1983). This showed that the $F\bar{4}3m$ assumption leads to a significantly superior fit to the experimental measurements especially at high angles and with reflexions having structure factors less than 10.0. The weak reflexions included nine that are forbidden under Fd3m symmetry and it was shown that the best atom positions led to satisfactory agreement between

observed and calculated structure factors in these cases.

1.4 Distortion mechanism

1.4.1 Introduction

As explained in Section 1.3.1, the Cr^{3+} ion in an octahedral environment would not be expected to be subject to the Jahn-Teller effect when in its normal electronic ground state. Confirmation of the latter may be obtained from measurements of magnetic susceptibility in the case of $MgCr_2O_4$ in which it is believed that the structural distortions are exceptionally marked. Such measurements have shown that the Cr^{3+} ion is indeed in its normal 'high spin' state (Lotgering, 1962). The Jahn-Teller mechanism for producing structure distortions is then eliminated in this case and, by analogy with the behaviour of small impurity ions in alkali halides, it was suggested by Grimes (1971) that the Cr^{3+} ion displcements might be produced through the local electrostatic potential conditions at the B-sites.

These ideas are supported particularly by the case of $ZnFe_2O_4$ where the calculations of Hudson and Whitfield (1967) and experimental studies of ^{57}Fe Mössbauer Spectrum by Evans et al (1971) showed that the potential at the

centre of an octahedral site is a maximum and thus by symmetry that there must be, in fact, two positions of minimum energy lying either side along a [111] axis through the site (Grimes, 1974). A large cation in such a situation (see Figure 1.5) would be held at the centre of symmetry through the repulsive interactions with neighbouring anions, but smaller cations such as Fe^{3+} or Cr^{3+} might be able to move nearer to positions of minimum energy and would thus become displaced off-centre (Grimes et al, 1971, 1972a).

1.4.2 Local atomic potential wells

For an atom in a real crystal, the potential energy will be the sum of the potential energies of interaction of that atom with every other atom of the solid and therefore in general must be composed of two parts: one long range and predominantly attractive, and the other a short range, repulsive component. The potential energy for a simple ionic solid, for example, might have the following form:

$$\phi(r) = \frac{-Ae^2}{4\pi\varepsilon_o r} + B \exp(-\frac{r}{\rho}) \qquad \ldots\ (1.1)$$

where r is the nearest neighbour separation, e is the electronic charge and A, B and ρ are constants. Here, the first term is Coulombic and attractive (the Madelung

Δ = Barrier height = $(14{\cdot}8 \pm 0{\cdot}5) \times 10^{-3}$ eV

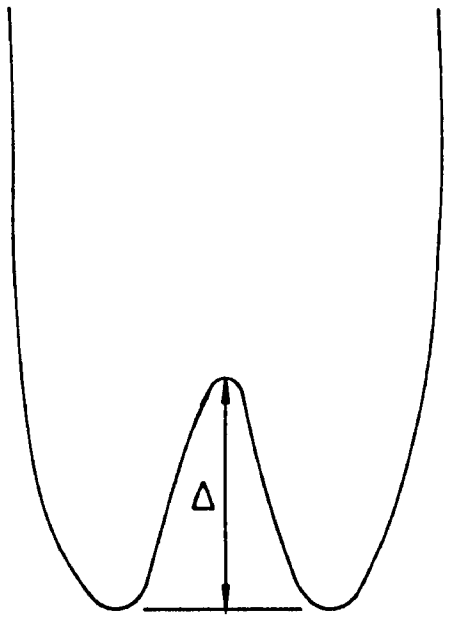

Figure 1.5 Potential energy distribution along a [111] axis through an octahedral site in $ZnFe_2O_4$ Spinel.

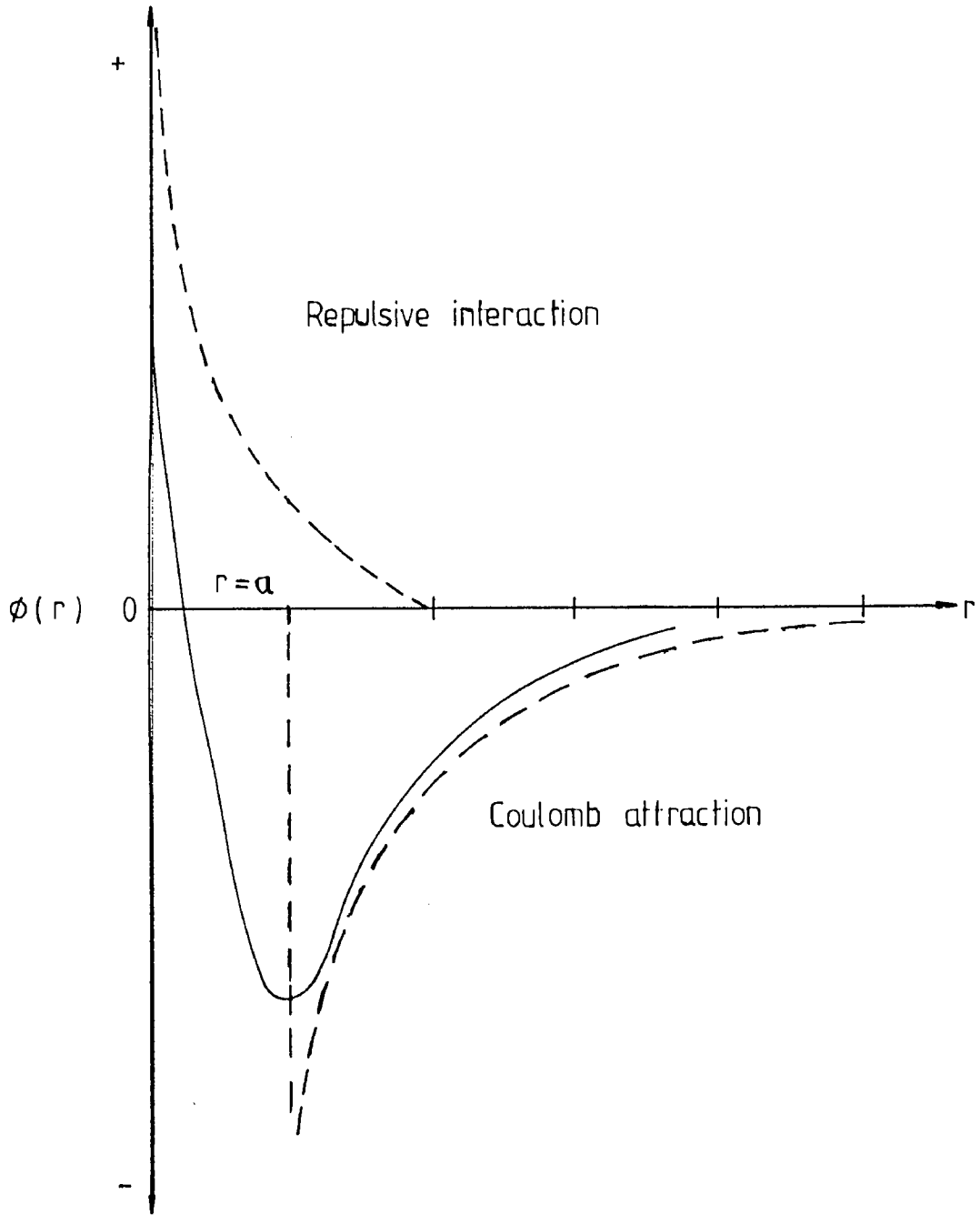

Figure 1.6 Potential energy of an ion in a crystal. The solid curve is the resultant of the sum of an attractive and repulsive component (both shown dotted)

energy), and the second, a repulsive Born-Mayer energy term which decreases very rapidly to negligible value with increasing r. Figure 1.6 shows the variation with r produced by adding these components, the total potential energy passing through a minimum value at r = a which corresponds to the equilibrium separation of the positive and negative ions in the crystal at 0K. With moderate amplitudes of vibration the significant part of the graph will be that in the neighbourhood of the minimum and, if this region is a good approximation to a parabola, the dynamic behaviour of the crystal will be closely represented by harmonic theory.

At high temperatures, however, the amplitude of vibration will be greater and also more asymmetric with respect to r = a. The deviation from the ideal parabolic curve may be represented by the expression:

$$\phi(r) = C(r-a)^2 - D(r-a)^3 - E(r-a)^4 \ldots\ (1.2)$$

where C, D and E are all positive coefficients which become successively smaller in magnitude. Discrepancies which are observed at higher temperatures between the measured values of physical properties and the values predicted by harmonic theory are then attributed to the presence of higher order terms.

1.4.3 Low temperature anharmonicity

The high temperature conditions described in Section 1.4.2 are not the only ones leading to anharmonicity. The existence of dipole moments owing to polarizability of some ions, or covalency, or, in the case of a metal, a free electron gas, introduces much more complex interactions. There are, in fact, a number of classes of materials for which the harmonic approximation is actually rather poor even at low temperatures. In some cases, it is now believed that the resultant $\phi(r)$ may have a form with off-centre valleys as shown in Figure 1.5, while in others the attractive and repulsive parts may cancel over an appreciable range to give a potential well which is locally quite flat (see Figure 1.7).

Examples of substances in which this kind of behaviour might occur have been reviewed by Dash et al (1968) and are thought to include ferroelectrics such as $BaTiO_3$, in which the Ti ions occupy wells with off-centre valleys, and high transition temperature superconductors like Nb_3Sn in which tin atoms occupy a flat-bottomed well (Shier and Taylor, 1967, 1968). Such materials exhibit acoustic relaxations (Testardi, 1972) and possess anomalous thermal expansion (Smith et al, 1975) and heat capacity behaviour (Knapp et al, 1975).

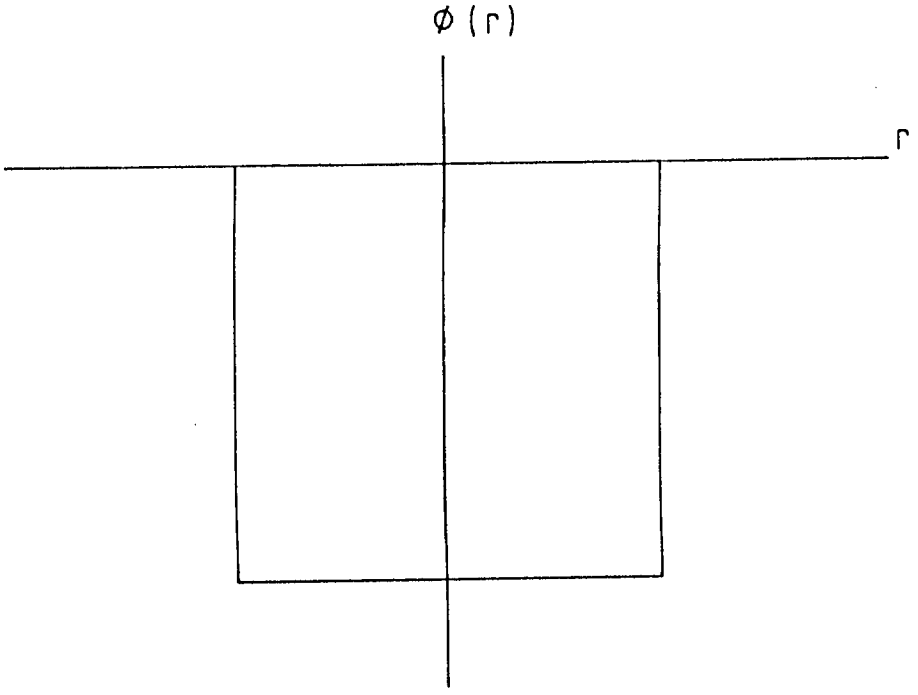

Figure 1.7 Potential well with locally flat centre at atomic site.

The evidence reviewed here indicates that the spinel compounds should be included among these anomalously anharmonic materials. It is worth noting, for example, that acoustic relaxations are common (Moran and Lüthi, 1969; Kino and Lüthi, 1971) while $ZnFe_2O_4$ exhibits a specific heat anomaly (Grimes, 1974).

In the metallic spinels, on the otherhand, the physical evidence indicates that off-centre ions do not occur (Williamson and Grimes, 1974) but instead superconductivity arises. In these compounds the local potential conditions have been shown to be similar to those in Nb_3Sn (Dawes et al, 1974) and significantly the compound $LiTi_2O_4$ has been shown to possess the highest transition temperature known among oxides (Matthias, 1975).

1.5 Scope of the present work

The discovery of the remarkable potential conditions at the octahedral sites in spinels and the subsequent discovery that the resulting atomic displacements produce an overall change of crystal symmetry naturally leads to comparisons with the behaviour of other anharmonic materials. The closest analogy is with compounds crystallizing with the zinc blende structure which also

conform to the cubic symmetry $F\bar{4}3m$ and with silicon and germanium. Such compounds show strong anharmonic effects (Dawson and Willis, 1967; Keating et al, 1971; Roberto et al, 1973, 1974) including unusual thermal expansion behaviour. Silicon, for example, has a negative coefficient of expansion at helium temperatures.

In the work to be described, attention has been concentrated on the thermal expansion behaviour of $MgAl_2O_4$ and $ZnFe_2O_4$. These materials were chosen because of the extensive additional information available. In the case of $MgAl_2O_4$, for example, the crystal structure is now known with very great detail (Grimes et al, 1983).

Finally, the existence of measurements of the heat capacities of these two compounds over an extensive range of temperature (King, 1955; Westrum and Grimes, 1957) provided the possibility of investigating the proportionality between heat capacity and thermal expansion. For a quasi-harmonic crystal the ratio

$$\gamma = 3\alpha V/\chi_S C_p = 3\alpha V/\chi_T C_v \qquad \ldots. \quad (1.3)$$

is a constant independent of temperature (Grüneisen, 1926, Appendix A). Here C_p and C_v are the molar heat capacity at constant pressure and volume respectively. χ_S and χ_T are the adiabatic and isothermal compressibility

respectively and V is the molar volume. In Chapter 5, the variation of γ with temperature for $MgAl_2O_4$ and $ZnFe_2O_4$ spinels is shown and discussed. These results are directly compared with the behaviour for silicon and germanium and also with corresponding results from the superconducting spinel $LiTi_2O_4$. Chapter 6 summarizes the conclusions and suggestions for further work.

CHAPTER 2

APPARATUS AND EXPERIMENTAL TECHNIQUE

2.1 X-ray diffractometer

The method chosen in this study for the determination of thermal expansion coefficients was based on the precision measurement of a crystal lattice parameter over a range of temperature using a well established X-ray diffraction technique. For these purposes a Philips powder diffractometer with low temperature attachments was used in conjunction with a stabilized X-ray generator. A simple schematic form and general view of the diffractometer are shown in Figure 2.1 and Figure 2.2. This equipment includes the following facilities:

(i) automatic continuous scanning across a range of angles 2θ (θ = Bragg angle), with output to a chart recorder in order to identify and assess the purity of the sample.

(ii) automatic fixed time step scanning across a selected diffraction line profile at different intervals of 0.01^{o}, 0.02^{o} and 0.05^{o} (2θ) with output to a printer or tape punch to record the intensity.

(iii) standard counting equipment including a pulse height

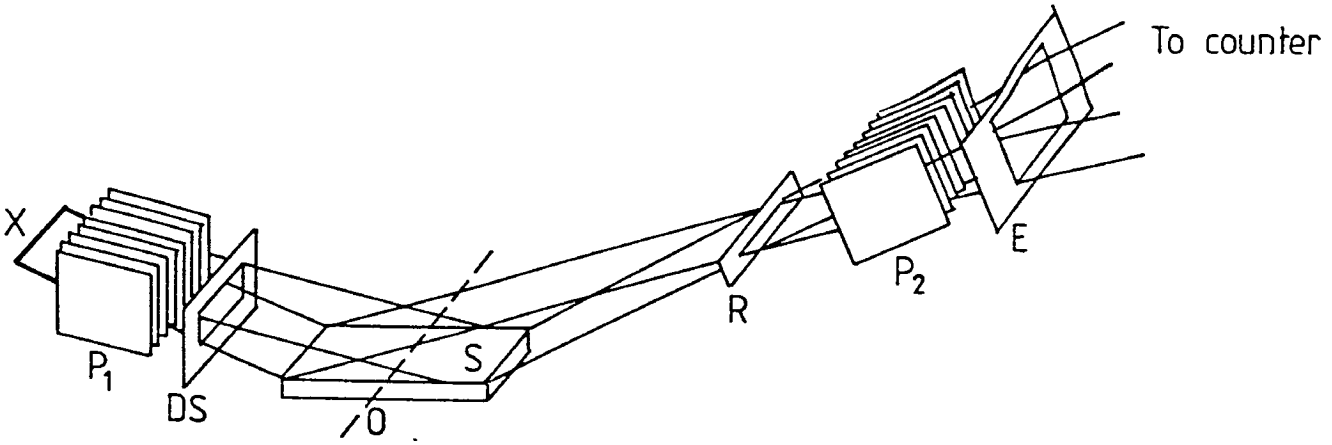

Figure 2.1 A typical powder diffractometer arrangement. X - focal line of x-ray tube, P_1 and P_2 - Soller slit assemblies, DS - divergence slit, O - goniometer axis of rotation, S - powder sample, E - anti-scatter slit, R - receiving slit. (after Parrish, 1965)

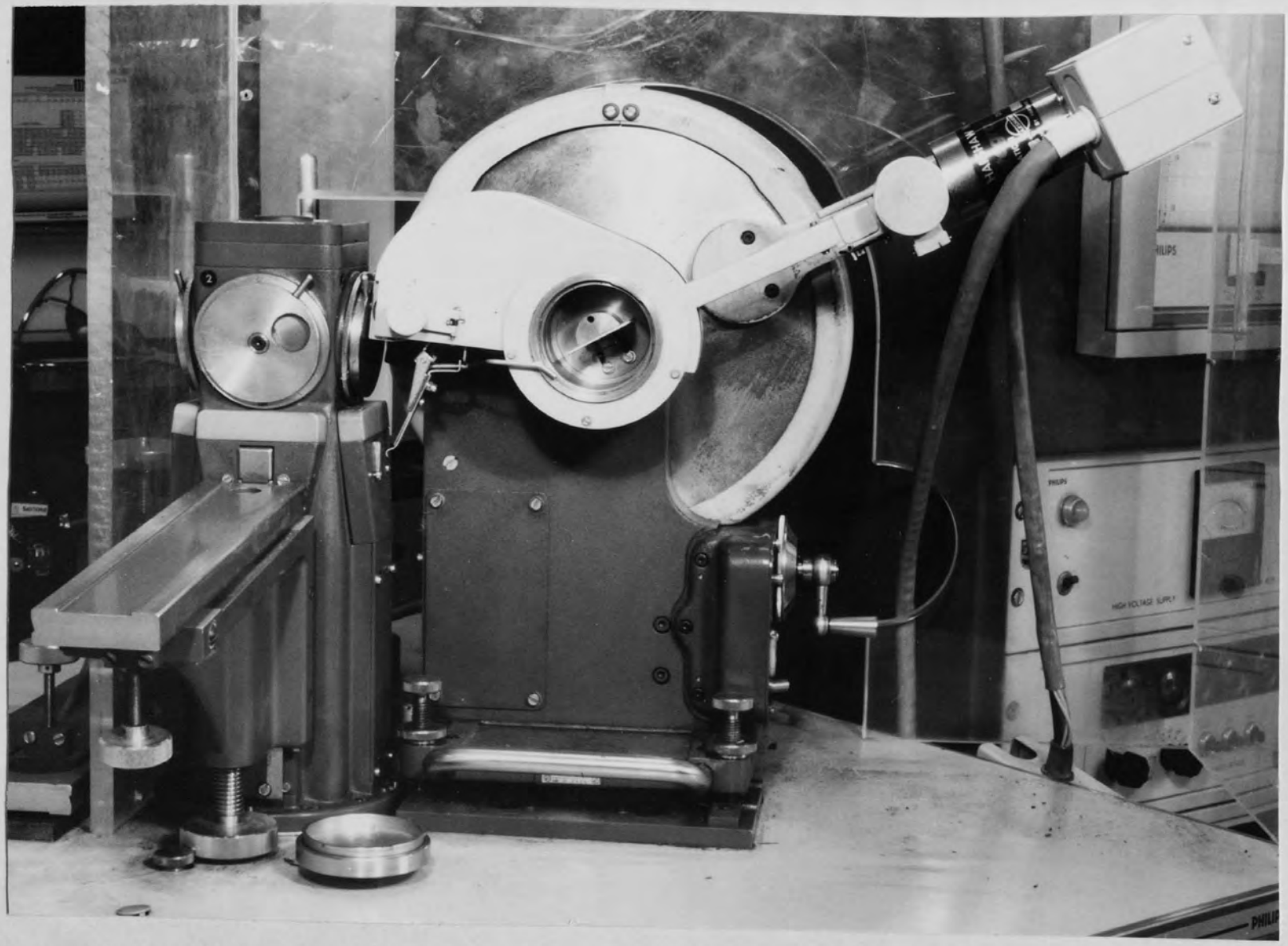

Figure 2.2 The Philips powder diffractometer

analyser which had to be calibrated in the following manner. First of all, the counter characteristic was determined by orientating the counter (Xenon proportional counter or NaI(Tℓ) scintillation counter) on the (220) line of silicon powder. Then the curve of applied voltage (volts or scale divisions) was plotted against count rate. The counter operating voltage was fixed at a value slightly greater than the beginning of the plateau. Finally the lower level and window settings of the pulse height analyser were adjusted to give the best signal intensity measurements.

The copper radiation (CuKα) with centroid wavelength, equal to 1.54178 A^{o} and the molybdenum radiation ($MoK\alpha_1$) with wavelength equal to 0.7093 A^{o} were used to determine the line positions of the spinel compounds.

There was a need to use filters to eliminate the CuKβ or MoKβ diffraction lines which tend to overlap with the tails of the lower orders of CuKα or MoKα respectively. In practice, two filters, one before and one after the sample holder, were used.

The diffractometer includes five slits, two soller slits with fixed values, a divergence slit, receiving slit and anti-scatter slit. The alignment of the X-ray beam and slits was carried out according to the procedure described

by Parrish (1965). Single and double knife edges were used for zeroing the receiving slit and 2:1 (2θ) settings respectively. The experimental conditions of the diffractometer systems are given in Table 2.1.

Each prepared sample was ground until the average particle size was between 30 and 60 μm. The ground sample was then pressed into the sample holder to decide the range over which to step-scan, a preliminary chart-recording of each profile of the sample was made and the intensity of the profiles obtained by the step scanning method.

For the intensity measurements of a selected high angle line, an interval of 0.02^{o} 2θ was used, while an interval of 0.01^{o} 2θ was used for a selected low angle line. It was found that a range of scan approximately ± 1.30^{o} 2θ about the centroid for the high angle and ±0.80^{o} 2θ about the centre of the low angle lines was sufficient.

2.2 Low temperature attachments

2.2.1 The cryostat

The X-ray diffractometer cryostat (Figure 2.3) operates on the principle of a controlled continuous transfer of liquid nitrogen from a storage vessel to the cryostat by

Radiation	1 - Cu Kα - Nickel filter 2 - Mo Kα - Zirconium filter
X-ray tube supply	1 - 40 KV, 20 mA 2 - 40 KV, 24 mA
Take-off angle	6°
Divergence slit	1°
X-ray source size	1.6 mm x 12 mm
Sample size	20 mm x 10 mm x 2 mm
Aperture of Soller-slits	2.25°
Receiving slit	0.1 mm
Source to sample distance	173 mm
Antiscatter slits	1°
X-ray counter	1 - Xenon proportional counter 2 - (NaI[Tℓ] Scintillation counter
Displacement of receiving slit from focussing circle	< 1 mm
Inclination of specimen plane to goniometer axis	Unknown, but small
Angular mis-setting of 2:1 ratio	Unknown, but small
Displacement of goniometer outside focussing circle	0.025 mm
Angular mis-setting of receiving slit	Unknown, but small
Angular mis-setting of centroid of X-ray beam	Probably < 0.25°

Table 2.1

Experimental conditions for the X-ray diffractometer

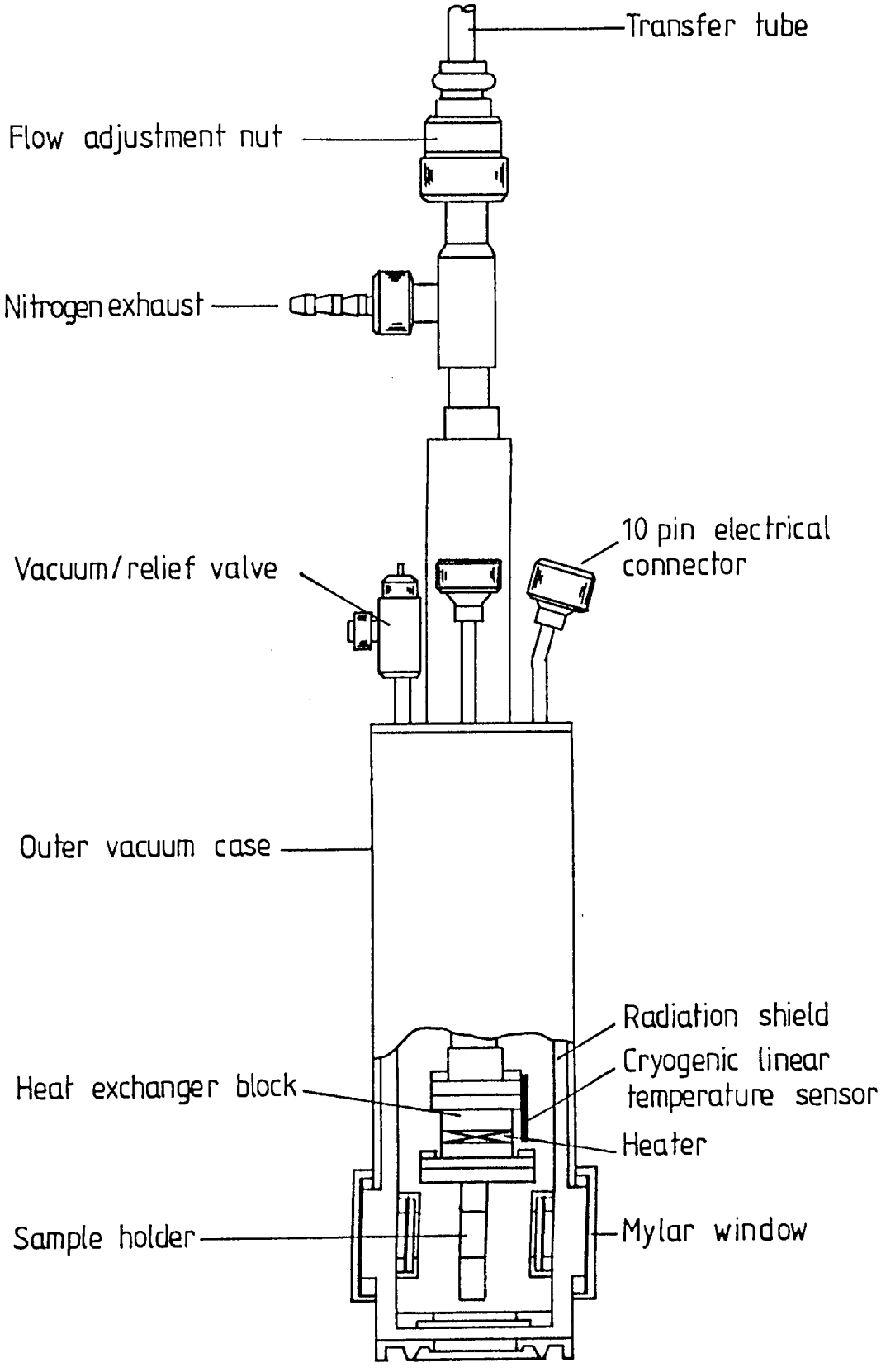

Figure 2.3 The cryostat

a transfer tube.

The top plate of the cryostat carries a pump-out valve, the two multiway electrical connections (10-way) and transfer tube entry.

To provide coarse and fine control of temperature with the temperature controller, the heat exchanger block is fitted with a 39 ohms heater, linear thermister and carbon resistor. Radiation shields are connected to the centre of the tube through a copper thermal link flange, to reduce the heat loads on the sample block. The temperature of the sample block may be maintained at any temperature between 77.0 K and room temperature by regulating the flow of liquid nitrogen through a flow control console.

The cryostat is provided with a window of aluminised 'Mylar' for minimum attenuation of the diffracted radiation. The form of the windows allows coverage of virtually all the back reflection region. An additional feature of this cryostat is the inclusion of an alignment slit in the specimen block which can be moved into position in the X-ray beam. This allows accurate alignment of the specimen surface with respect to the X-ray beam. The position of the (220) line of silicon powder was used to check the alignment. Finally, the

alignment was checked again before taking measurements on a spinel sample at low temperatures by comparing a chart scan at room temperature with the cryostat fitted, to the corresponding scan at room temperature in the absence of the cryostat.

2.2 The flow control console

The flow of the coolant from the storage vessel through the transfer tube to the cryostat was regulated by a flow control console (Figure 2.4). The entry to this unit from the cryostat leads initially to a circulating pump via a needle valve mounted in series. The exit gas from the circulating pump is brought back to the console to pass through a flow meter. The flow meter gives the liquid nitrogen consumption of cm^3/hr.

2.2.3 Transfer tube

The transfer tube connects the cryostat to the liquid gas reservoir. It is made of two metal parts connected by a 90^o flexible coupling and is fitted with a pump out valve. The temperature of the sample could be lowered by adjustment of the flow through the transfer tube and adjustment of the needle valve on the control console.

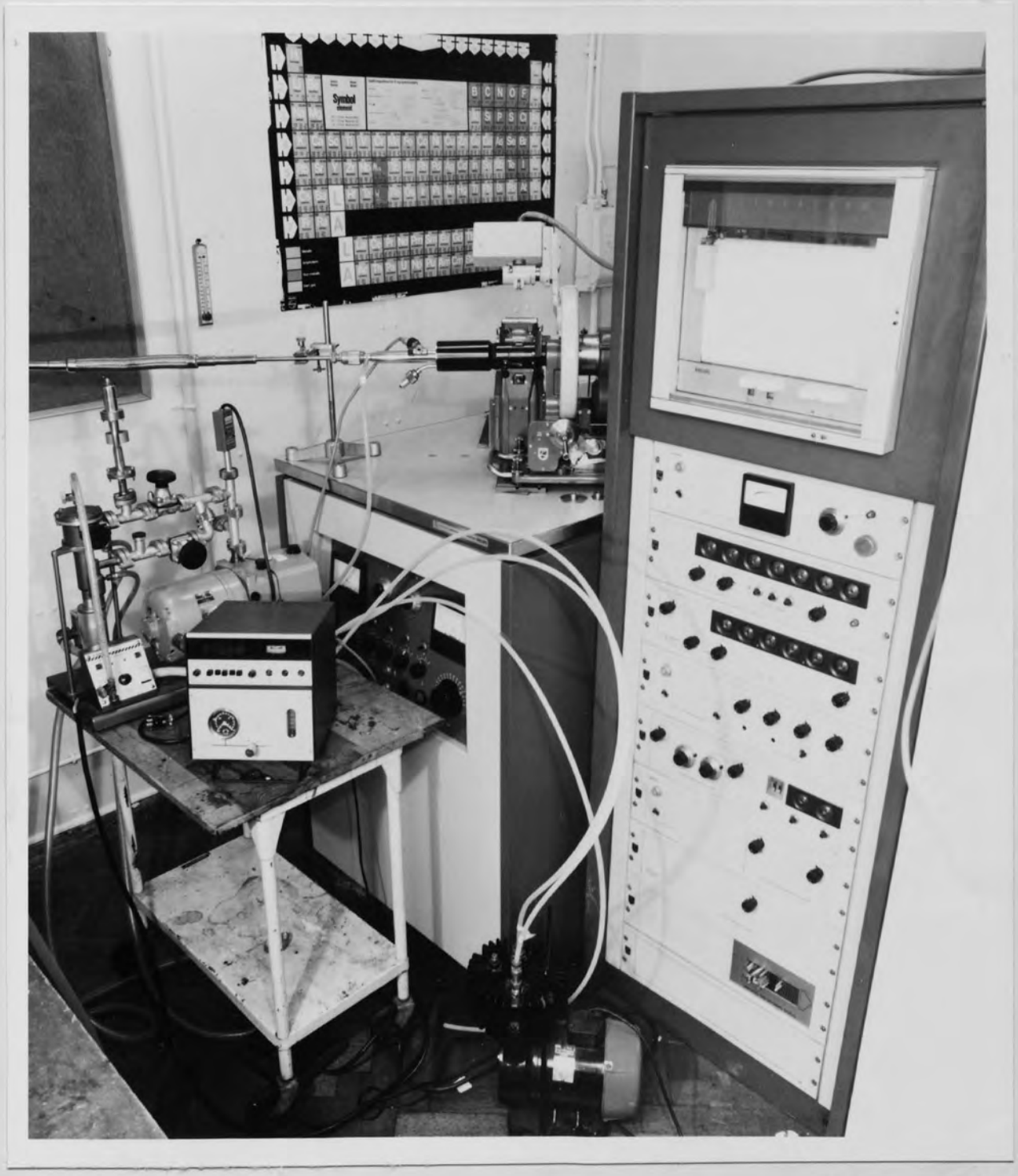

Figure 2.4 General view of the low temperature equipment

2.2.4 The vacuum system

The equipment used was a diffusion pump with cold trap, backed by a rotary pump to produce a pressure equal to 10^{-5} torr which is important for removing any moisture which may accumulate in the cryostat.

2.2.5 The temperature controller

The Oxford continuous flow cryostat is supplied with a cryogenic linear temperature sensor (CLTS). This is a small surface thermometer gauge consisting of three sensing grids. These are laminated into an epoxy resin matrix and connected electrically in series. The two alloys are special grades of nickel and manganin. The linear temperature sensor is fabricated with integral printed circuit terminals to provide strong, convenient attachment points for the lead wire system. Because of its low thermal mass and large contact area, the CLTS accurately and quickly responds to the temperature change in the surface to which it is bonded. The resistance of the CLTS is 290 ohms at 300 K and had been shown by calibration to decrease linearly with temperature reaching a value of 220 ohms at 4.2 K. The temperature of the sample could be maintained within ± 0.5 K over the low temperature range.

2.3 Determination of diffraction line positions and lattice parameters

In Bragg's law, the wavelength is single valued and subject to diffraction by a crystal with a unique interplanar distance d. This implies that a diffraction maximâ would be observed with negligible width at an angle 2θ with respect to the direction of the primary beam. In practice, diffraction line profiles are observed to spread over a range of angles in the neighbourhood of the angle 2θ , chiefly because of the finite width of the characteristic emission lines. However, other contributions can be significant, arising from both instrumental and diffraction sources. To reduce this effect, the width of the slits could be reduced, but this reduces the intensity to be detected, thus a compromise has to be made.

Accurate lattice parameters were determined using the centroid (Pike and Wilson, 1959) as a measure of diffraction line position. This measure has the advantages of being statistically accurate and easily corrected for the effects of instrumental aberrations (Wilson, 1963). The latter fall into two groups, namely physical and geometrical aberrations. The first must be calculated for each centroid and added or subtracted directly. The second group may be removed by

extrapolation techniques. However, it has been found that the corrections of the first kind cancel at high angles (approximately $2\theta = 100^{o}$ up to 150^{o}) and the extrapolation terms for the second kind (i.e. $Cot^{2}\theta$ and $Cos\theta Cot\theta$) tend to zero, as θ tends to 90^{o}. Thus, for the spinel peaks which occur at approximately 130^{o} 2θ the geometrical and physical aberrations are negligible in comparison to random errors in measuring the angle, as shown in Figure 2.5 (Cheary, 1971).

Finally, a value for the lattice parameter, a, could be determined from the centroid angle θ_c using a centroid wavelength which in this study was taken to be the weighted mean of the $K\alpha_1$ and $K\alpha_2$ wavelengths. We used $a = d\sqrt{h^2 + K^2 + \ell^2}$ with $d = \lambda_c/2\sin\theta_c$ and

$$\lambda_c = (2\lambda_{K\alpha_1} + \lambda_{K\alpha_2})/3 \qquad \ldots\ (2.1)$$

With $ZnFe_2O_4$, $MoK\alpha_1$ radiation was used and in this case the line positions used occurred at a lower angle where the instrumental aberrations are not negligible. However, the use of an internal standard (see Section 2.4) provided an effective calibration.

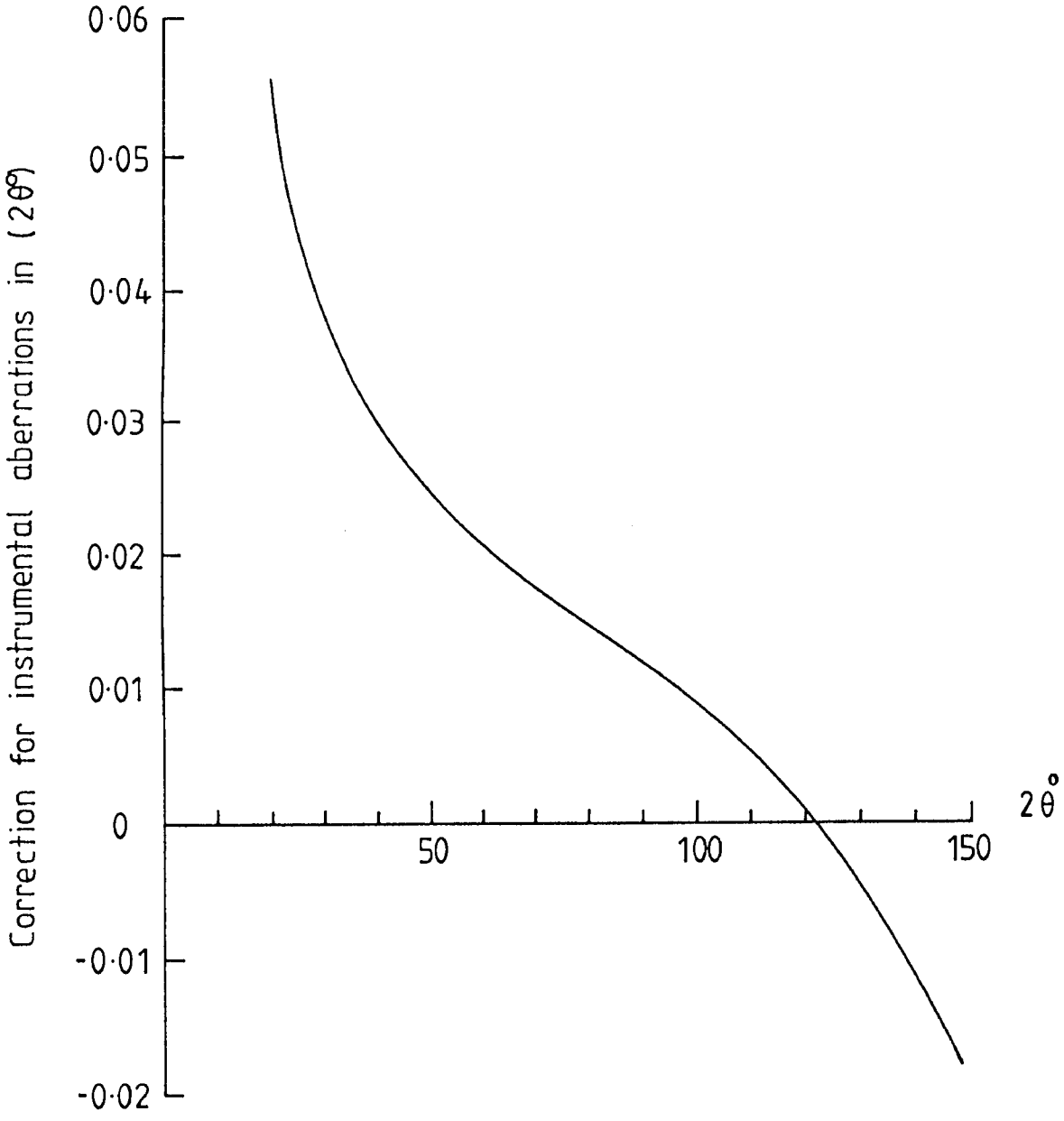

Figure 2.5 Centroid correction for instrumental aberrations. (after Cheary, 1971)

2.4 Use of an internal standard

Because in this study measurements of lattice parameters were to be made over a range of temperature, errors arise from temperature measurements as well as from aberrations in the diffraction process. The thermometer had been calibrated (see Section 2.2.5) but as an additional check it seemed desirable to incorporate an internal standard. This was achieved by using as diffraction specimen a fine mixture of the spinel compound to be investigated, together with a pure element with well known lattice parameter and thermal expansion behaviour for the temperature range concerned.

Two other factors were of importance. Firstly, the element concerned should ideally have a simple crystal structure, i.e. a diffraction pattern with few lines. Secondly, such lines as occur should appear between lines corresponding to the spinel phase.

2.5 Experimental procedure at low temperature

Before making measurements it was necessary to check the alignment of the diffractometer system including the low temperature attachements at both room and low temperatures. At the same time the identity of the

prepared spinel compounds was checked from a recording of the line profiles at room temperature. The intensities of the chosen internal standard lines were checked to determine whether they were of an acceptable intensity compared to the background intensity and if this was not the case a different mixture of the chosen internal standard with the spinel compound was tested until the best intensity ratios were achieved. Finally, the mixture of the spinel and its internal standard was cooled to liquid nitrogen temperature.

Each time the liquid nitrogen vessel was filled to maintain continuous flow, it was necessary to wait at least one hour in order to achieve an equilibrium temperature. When the temperature settled at the required level within ± 0.5 K, the intensities of the chosen internal standard and the spinel compound lines were measured at an interval of 0.01^{o} 2θ or 0.02^{o} 2θ with simultaneous output to a printer every 200 seconds. The temperature was then increased by approximately another 10 K. This process was repeated until room temperature was reached when the intensity measurements were repeated.

The time required to collect a complete spectrum from a given spinel sample and internal standard was approximately seven weeks.

After collection of the data, the line positions for certain selected diffraction peaks were determined and the lattice parameters for the spinel compound over a range of temperatures calculated and then corrected using the internal standard. The temperature variation of these corrected values for the lattice parameters was smoothed by fitting a polynomial function in T through the experimental data.

2.6 Determination of the linear coefficient of thermal expansion

The thermal expansion values for spinel compounds were determined using the lattice parameters smoothed by fitting a polynomial function in temperature T of the third degree through the experimental results

$$a_T = a_o + a_1 T + a_2 T^2 + a_3 T^3 \quad \ldots\ldots (2.2)$$

where a_T is the lattice parameter at TK and a_0, a_1, a_2 and a_3 are constants. The corresponding coefficient of thermal expansion, α_T, can be calculated by differentiating the above polynomial equation with respect to temperature (T) then dividing by the lattice parameter at that temperature, a_T,

$$\alpha_T = \alpha_0 + \alpha_1 T + \alpha_2 T^2 \quad \ldots\ldots (2.3)$$

where α_0, α_1, and α_2 are constants, related to a_1, a_2 and a_3 respectively.

2.7 Experimental errors

One advantage which the X-ray technique shares with the optical interferometric technique over other methods lies in the aboslute nature of the thermal expansion coefficients to which it leads. A second advantage lies in the fact that it gives a measure of expansion uncomplicated by dimensional changes resulting from vacancy formation, from the presence of impurities, or from any other cause. Offsetting these advantages to some extent is the fact that the sensitivity is not generally as high as those of some of the other methods (Yates, 1972). The usual resolution for changes in lattice parameter, a, is $\Delta a/a \cong 10^{-5}$. This is sensitive enough for determining α at temperature $T > \theta_D/10$, (Barron et al, 1980).

In practice, the precision with which a lattice parameter can be measured depends primarily on the precision with which the diffraction line positions can be measured, for the uncertainty in the wavelength of a characteristic

X-ray line is virtually fixed. More importantly for the present work, is the fact that, in principle, a thermal expansion coefficient, α, is calculated from the small difference in lattice parameter which occurs as a result of a small change in temperature, i.e. the uncertainty in α is inherently large because nearly equal quantities have to be subtracted.

This problem was minimised, firstly by using an internal standard (see Sections 2.4, 3.2 and 4.3) and secondly by deriving thermal expansion coefficients from a smoothed curve drawn through the experimental lattice parameter data over the whole temperature range investigated. As a result of these procedures the possible error in lattice parameter at any given temperature was reduced to about $\pm$ 0.00011 Å and $\pm$ 0.00025 Å for $MgAl_2O_4$ and $ZnFe_2O_4$ respectively.

The size of the temperature drift was usually $\pm$ 0.2 K, but in the worst cases it was $\pm$ 0.5 K so that the uncertainty in temperature is considered to be $\pm$ 0.5 K. This uncertainty is larger than the precision of the sensor and this produced uncertainty of the order of 1% for α values at 80 K decreasing to 0.2% at room temperature.

CHAPTER 3

RESULTS FOR $MgAl_2O_4$ SPINEL

3.1 Preparation of $MgAl_2O_4$

There are a number of different methods of producing polycrystalline spinel oxides and these are reviewed in detail by Standley (1972). The mixed oxide method of preparation was used to prepare $MgAl_2O_4$. Essentially this process involves mixing of appropriate quantities of the pure component oxides, and firing of the mixture at a high temperature, usually after hydraulic pressing into suitable compacts. The firing stages are particularly critical for obtaining the right proportions of metal ions of the correct valency in the final product and careful control of the furnace atmosphere both at temperature and during cooling can be vital.

To prepare $MgAl_2O_4$, oxides of magnesium and aluminium were mixed according to the formula:

$$MgO + Al_2O_3 \rightarrow MgAl_2O_4$$

These oxides were chemically pure (99.9%) and finely powdered (Supplier Koch-Light & Co). These were ground

Figure 3.1 Apparatus for the preparation of pellets

together using a mortar and a pestle until visual homogeneity was achieved. To obtain better results, the mixing was continued for another three hours in a mechanical mixer. This ground mixture was loaded into a steel press with 15 mm diameter polished dies (Figure 3.1) and was compressed into pellets in a hydraulic press under seven tons of pressure. The furnace used to fire the pellets was a PCA TAS furnace(Figure 3.2) having a 96 mm 'hot zone'.After ensuring that the pellets were in the centre of the hot zone, the temperature of the furnace was allowed to rise to the required value, by means of the temperature controller to within an accuracy of ± 20 K. The pressed pellets were then fired in an oxygen atmosphere first at 1100 K for twenty four hours to obtain an initial reaction between the component oxides and then at a higher temperature.The final stage involved refiring first at 1300 K and then at 1700 K in each case for another twenty four hours (the sample was reground and repressed between consecutive firings to achieve good grain size for the spinel phase). It was found, in general, that the reaction was incomplete at 1300 K, the result was mainly spinel phase but small amounts of the constituent oxide phases were present as well. However, good purity results were achieved at 1700 K. The resulting white compound was identified with X-ray powder photographs using copper radiation, and the results are shown in Table 3.1.

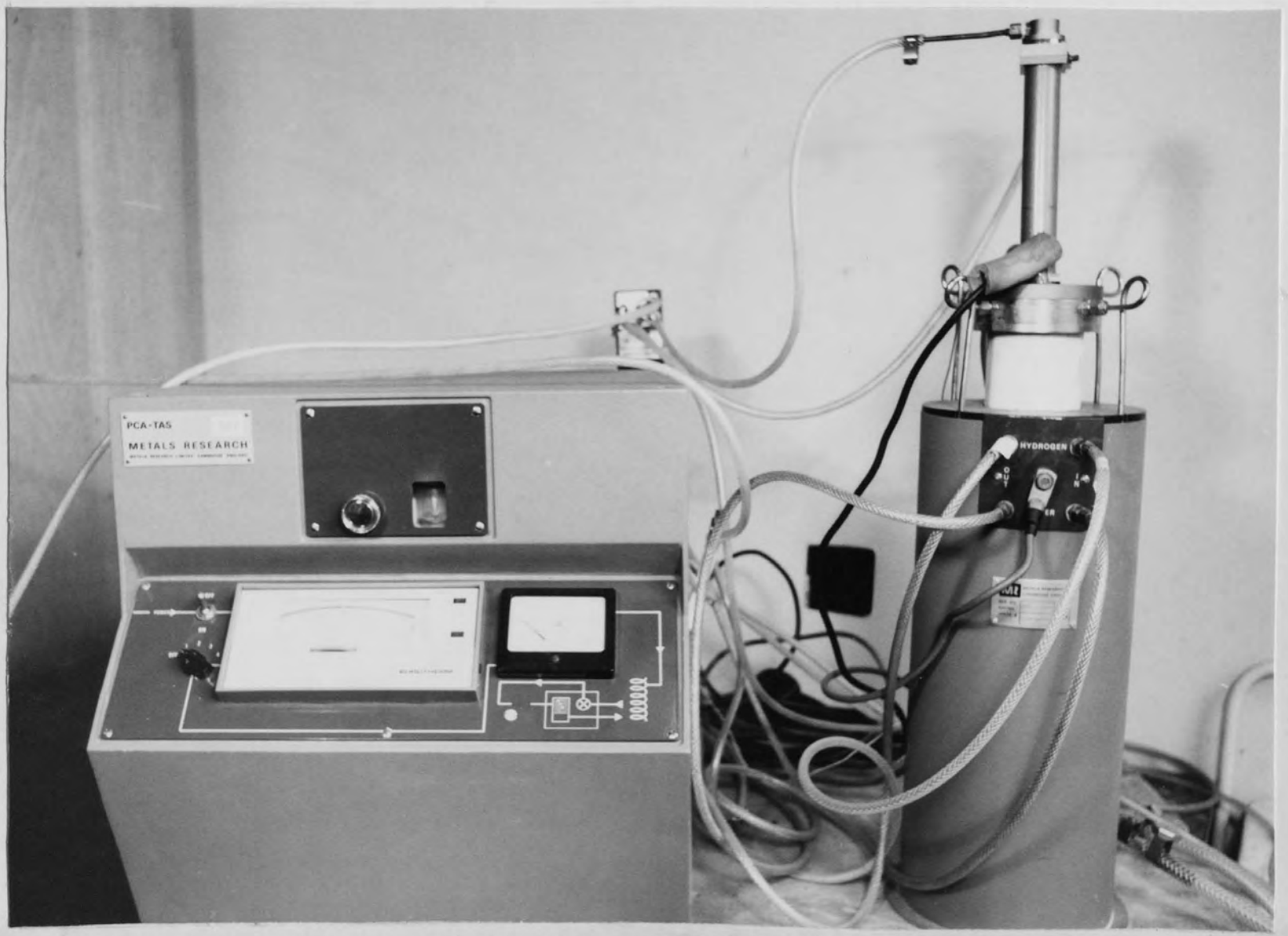

Figure 3.2 Furnace used for the preparation of spinel

Index (hkl)	Interplanar distance d/A°	Relative intensity I/Imax	Approximate angular position in 2θ°
111	4.66	40	19.20
220	2.86	30-40	31.31
311	2.44	100	36.90
222	2.33	V Faint	38.60
400	2.03	60	44.87
422	1.66	10	55.73
511 (333)	1.56	50	59.44
440	1.43	60-70	65.33
531	1.38	V Faint	68.73
620	1.28	V Faint	74.23
533	1.23	10	77.46
622	1.22	V Faint	78.53
444	1.16	10	82.76
711 (551)	1.13	V Faint	85.90
642	1.08	Faint	91.10
731 (553)	1.05	10	94.25
800	1.01	5	99.51
822	0.95	V Faint	108.40
751 (555)	0.93	10	111.34
840	0.90	5	117.50
931	0.85	10	130.97
844	0.82	20	140.14

Table 3.1

X-ray data for $MgAl_2O_4$ spinel used to check against the A.S.T.M. index

3.2 Choice of internal standard

The essential characteristics for an internal standard were reviewed in Section 2.4. Materials which have these characteristics are typically elements and for $MgAl_2O_4$ possible standards were Si, Ag and Ge. Of these three, Si was found to have certain advantages over the other two. Firstly, there is much published data of expansivity and thermal expansion coefficients over the temperature range between liquid helium and high temperature (Gibbons, 1958; Carr et al, 1965; Batchelder and Simmons, 1965; Lyon et al, 1977; White, 1973). Moreover, the Si expansivity is relatively small; so it is useful as a standard for the measurements of low expansivity materials, as well as high expansivity materials. Secondly, it has a high melting point and hence can be used over a wide temperature range. Due to its technological importance, very high purity Si can be obtained. Finally, Si gives diffraction lines close to those of $MgAl_2O_4$ spinel, particularly at the high angle range where the physical and geometrical aberrations are negligible (Wilson, 1963).

Different proportions of $MgAl_2O_4$ spinel and Si were tried, and it was found that a mixture of 70% of $MgAl_2O_4$ spinel with 30% of Si gave the best intensity results for the chosen diffraction lines.

Table 3.2 presents the published expansivity and lattice parameter measurements for Si over the temperature range 77.5 to 300.1 K (Batchelder and Simmons, 1965).

3.3 Correction method

The diffracted intensity distribution for the spinel-silicon mixture in the high Bragg angle region is shown in Figure 3.3. The most suitable diffraction lines for the lattice parameter determination of the spinel were (751) and (931). In this region there are also two good lines from Si, namely (531) and (620) and these, therefore, were used to correct the measured centroids of the spinel phase. Note that although the temperature was measured by a calibrated thermometer the use of Si as an internal standard provides an additional check.

The centroid positions derived from the silicon spectrum $\theta_c(531)$ and $\theta_c(620)$ are summarized in Table 3.3 and these were used to calculate experimental d spacings and hence corrections $\Delta\theta_c(531)$ and $\Delta\theta_c(620)$ in accordance with Bragg's law $2d\sin\theta_c = \lambda_c$, i.e. $\Delta\theta_c = \frac{-\Delta d}{d\cot\theta_c}$ (see Table 3.4). The correction $\Delta\theta_c(531)$ was used to correct the centroid position of the neighbouring spinel line (751) and similarly $\Delta\theta_c(620)$ was used to correct (931) from spinel.

TEMPERATURE (K)	Δ a/a' x 10^5	$a_{calc.}$ (Å)
77.5	-17.69	5.42948
89.6	-18.37	5.42944
99.6	-19.39	5.42938
110.3	-18.59	5.42943
120.0	-19.23	5.42939
130.0	-19.07	5.42940
140.0	-18.82	5.42942
150.0	-18.28	5.42944
160.0	-17.72	5.42948
171.1	-17.13	5.42951
180.9	-16.29	5.42955
189.8	-14.96	5.42963
199.8	-13.45	5.42971
210.3	-12.35	5.42977
220.1	-10.69	5.42986
230.3	-9.16	5.42994
240.0	-7.58	5.43003
250.0	-5.30	5.43015
259.6	-3.27	5.43026
270.1	-0.72	5.43040
300.1	+6.95	5.43082

Table 3.2

Expansivity and lattice parameter measurements for silicon according to Batchelder and Simmons (1965) with a' = 5.43044 Å (lattice parameter of silicon at 273.15 K)

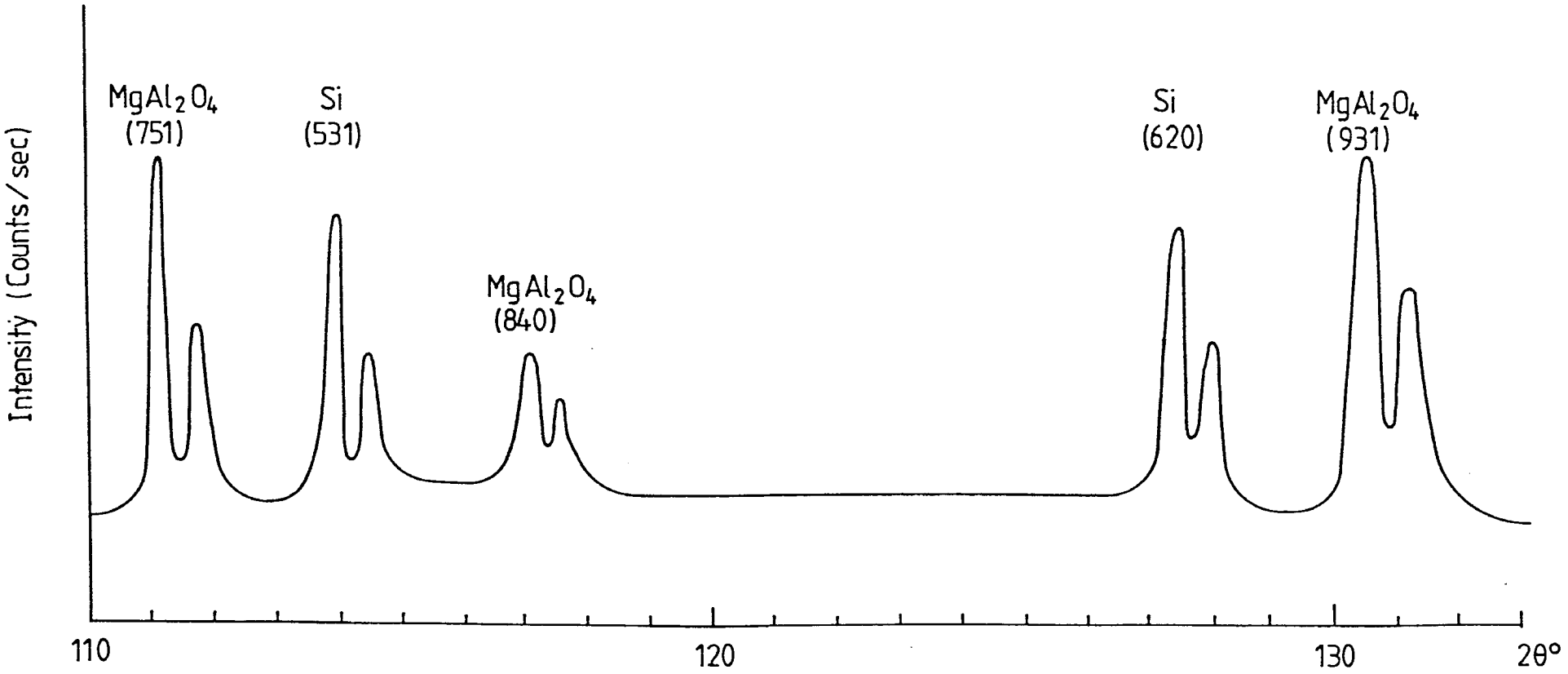

Figure 3.3 The diffracted intensity distribution for the spinel - silicon mixture in the high Bragg angle region.

TEMPERATURE (K)	θ_c(531) (°)	θ_c(620) (°)
77.5	57.104	63.868
89.6	57.110	63.872
99.6	57.104	63.869
110.3	57.102	63.859
120.0	57.097	63.861
130.0	57.095	63.861
140.0	57.093	63.858
150.0	57.098	63.855
160.0	57.093	63.858
171.1	57.096	63.858
180.9	57.088	63.851
189.8	57.088	63.853
199.8	57.078	63.849
210.3	57.083	63.843
220.1	57.083	63.843
230.3	57.078	63.843
240.0	57.083	63.843
250.0	57.076	63.847
259.6	57.073	63.833
270.1	57.088	63.944
300.1	57.072	63.823

Table 3.3

Measured centroid Bragg angles for the (531) and (620) lines of silicon

TEMPERATURE (K)	$\Delta\theta_c^{\circ}(531) \times 10^{-4}$	$\Delta\theta_c^{\circ}(620) \times 10^{-4}$
77.5	5.9	4.5
89.6	5.0	3.9
99.6	6.2	4.5
110.3	6.4	6.1
120.0	7.4	6.0
130.0	7.7	5.9
140.0	8.0	6.5
150.0	7.0	6.8
160.0	7.8	6.2
171.1	7.2	6.0
180.9	8.5	7.1
189.8	8.3	6.4
199.8	9.8	6.8
210.3	8.8	7.6
220.1	8.5	7.4
230.3	9.1	7.1
240.0	8.0	6.8
250.0	8.9	5.6
259.6	9.1	7.7
270.1	6.1	5.1
300.1	7.7	7.2

Table 3.4

Line position corrections found from Si (531) and (620) lines respectively

3.4 Determination of lattice parameters as a function of temperature

The measured centroid Bragg angles for (751) and (931) diffraction lines from $MgAl_2O_4$ spinel over the temperature range 77.5 to 300.1 K are summarized in Table 3.5. The corresponding lattice parameters obtained when these values were corrected and used with the centroid wavelength of CuKα radiation (1.54178 A^o) are shown in columns two and three of Table 3.6, ($a_{corrected}(751)$ and $a_{corrected}(931)$). The average of these lattice parameters for $MgAl_2O_4$ ($a_{ave.}$) are presented in column four and finally, column five presents the smoothed values (a_{smooth}) which result from fitting a polynomial equation of the third degree in temperature T through the average lattice parameters (Figure 3.4). The constant coefficients in the polynomial in T which gave the best fit to the experimental data were found to be

$$a_0 = 8.0741 \pm 0.0001 \ (A^o)$$

$$a_1 = 0.571 \times 10^{-5} \ (A^o)$$

$$a_2 = 0.730 \times 10^{-7} \ (A^o)$$

$$a_3 = 0.2086 \times 10^{-10} \ (A^o)$$

The root mean square deviation of the smoothed values from the experimental values was found to be 0.00011 A^o which could be taken as a measure of the precision of the lattice parameter results for the temperature range covered.

TEMPERATURE (K)	θ_c(751) °	θ_c(931) °
77.5	55.738	65.590
89.6	55.745	65.598
99.6	55.734	65.588
110.3	55.733	65.576
120.0	55.728	65.577
130.0	55.725	65.574
140.0	55.722	65.568
150.0	55.719	65.567
160.0	55.720	65.563
171.1	55.720	65.562
180.9	55.710	65.551
189.8	55.710	65.548
199.8	55.703	65.545
210.3	55.701	65.538
220.1	55.698	65.532
230.3	55.694	65.527
240.0	55.695	65.527
250.0	55.689	65.521
259.6	55.681	65.515
270.0	55.698	65.515
300.1	55.670	65.486

Table 3.5

Measured centroid Bragg angles for the (751) and (931) lines of $MgAl_2O_4$

TEMPERATURE (K)	a_{corr} (751) (A°)	a_{corr} (931) (A°)	a_{ave} (A°)	a_{smooth} (A°)
77.5	8.07465	8.07405	8.07435	8.07415
89.6	8.07441	8.07377	8.07409	8.07424
99.6	8.07481	8.07413	8.07447	8.07433
110.3	8.07473	8.07443	8.07458	8.07445
120.0	8.07473	8.07433	8.07453	8.07457
130.0	8.07482	8.07452	8.07467	8.07471
140.0	8.07498	8.07470	8.07484	8.07486
150.0	8.07586	8.07462	8.07524	8.07504
160.0	8.07525	8.07518	8.07522	8.07523
171.1	8.07560	8.07530	8.07545	8.07546
180.9	8.07577	8.07567	8.07572	8.07568
189.8	8.07595	8.07595	8.07595	8.07589
199.8	8.07586	8.07614	8.07600	8.07615
210.3	8.07654	8.07624	8.07639	8.07644
220.1	8.07698	8.07680	8.07689	8.07672
230.3	8.07690	8.07719	8.07705	8.07704
240.0	8.07759	8.07729	8.07744	8.07735
250.0	8.07759	8.07805	8.07782	8.07770
259.6	8.07829	8.07767	8.07798	8.07804
270.1	8.07829	8.07863	8.07846	8.07844
300.1	8.08010	8.07967	8.07989	8.07969

Table 3.6

Lattice parameter results for $MgAl_2O_4$

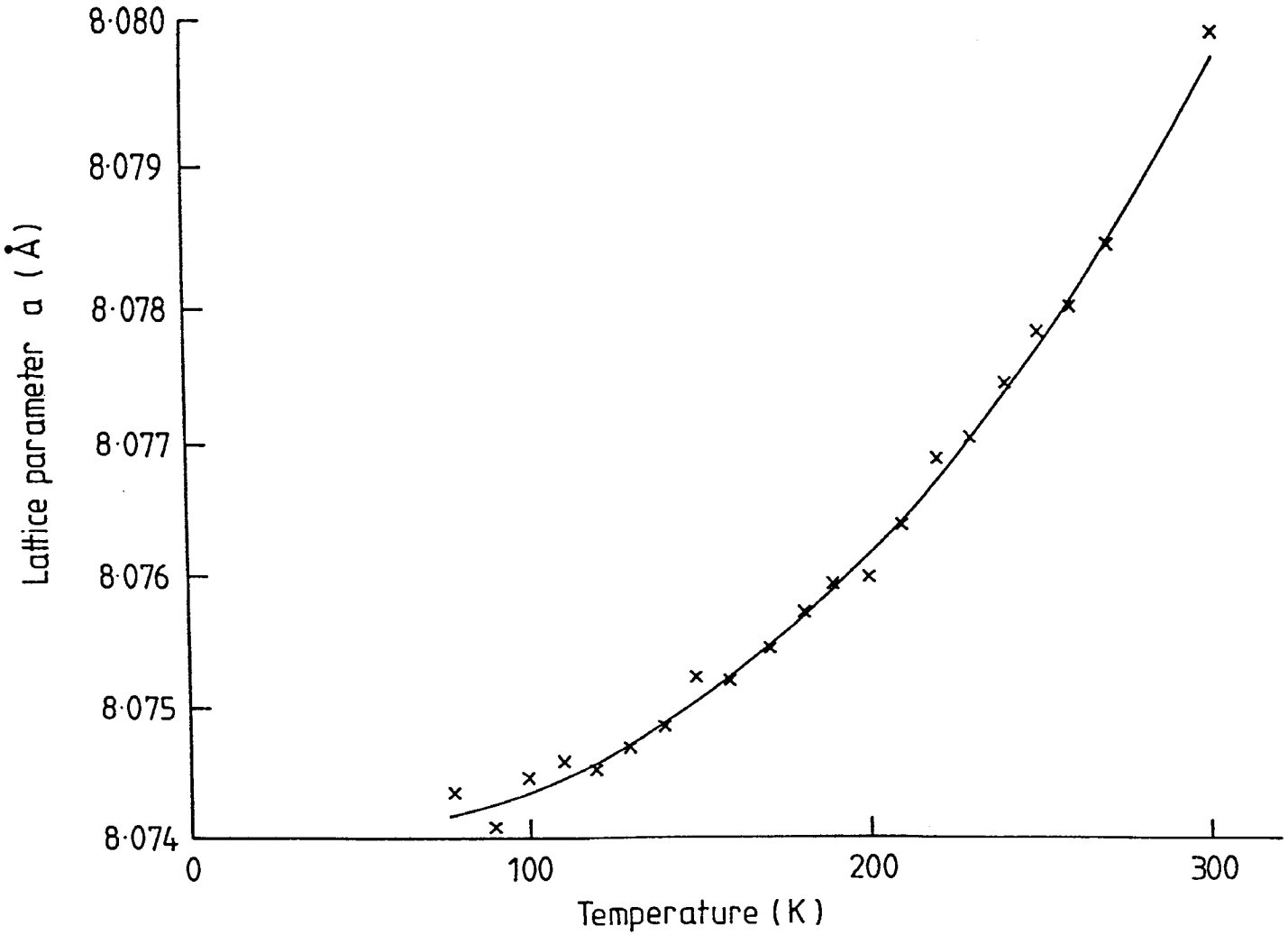

Figure 3.4 The averaged values of lattice parameters for $MgAl_2O_4$ compared with the smoothed curve as a function of temperature.

3.5 Determination of thermal expansion coefficients as a function of temperature

The values of linear coefficients of thermal expansion, α, over the temperature range 77.5 to 300.1 K (Table 3.7) were calculated using Equation 2.3 with constants derived from a_1, a_2 and a_3 as described in Section 3.4. Therefore,

$$\alpha_o = 0.571 \times 10^{-5}/a_T$$

$$\alpha_1 = 1.46 \times 10^{-7}/a_T$$

$$\alpha_2 = 0.6258 \times 10^{-10}/a_T$$

As $MgAl_2O_4$ is a cubic material, the volume coefficients of thermal expansion β may be found by using the relationship $\beta = 3\alpha$.

Figure 3.5 shows the variation of α with temperature and it was found that the value of α at 300.1 K is $5.48 \times 10^{-6}K^{-1}$.

Temperature (K)	Linear Coefficients of Thermal Expansion α (10^{-6} K^{-1})
77.5	0.81
89.6	1.04
99.6	1.24
110.3	1.45
120.0	1.64
130.0	1.84
140.0	2.04
150.0	2.25
160.0	2.45
171.1	2.68
180.9	2.88
189.8	3.07
199.8	3.28
210.3	3.50
220.1	3.71
230.3	3.93
240.0	4.14
250.0	4.36
259.6	4.57
270.1	4.81
300.1	5.48

Table 3.7

Linear coefficients of thermal expansion for $MgAl_2O_4$

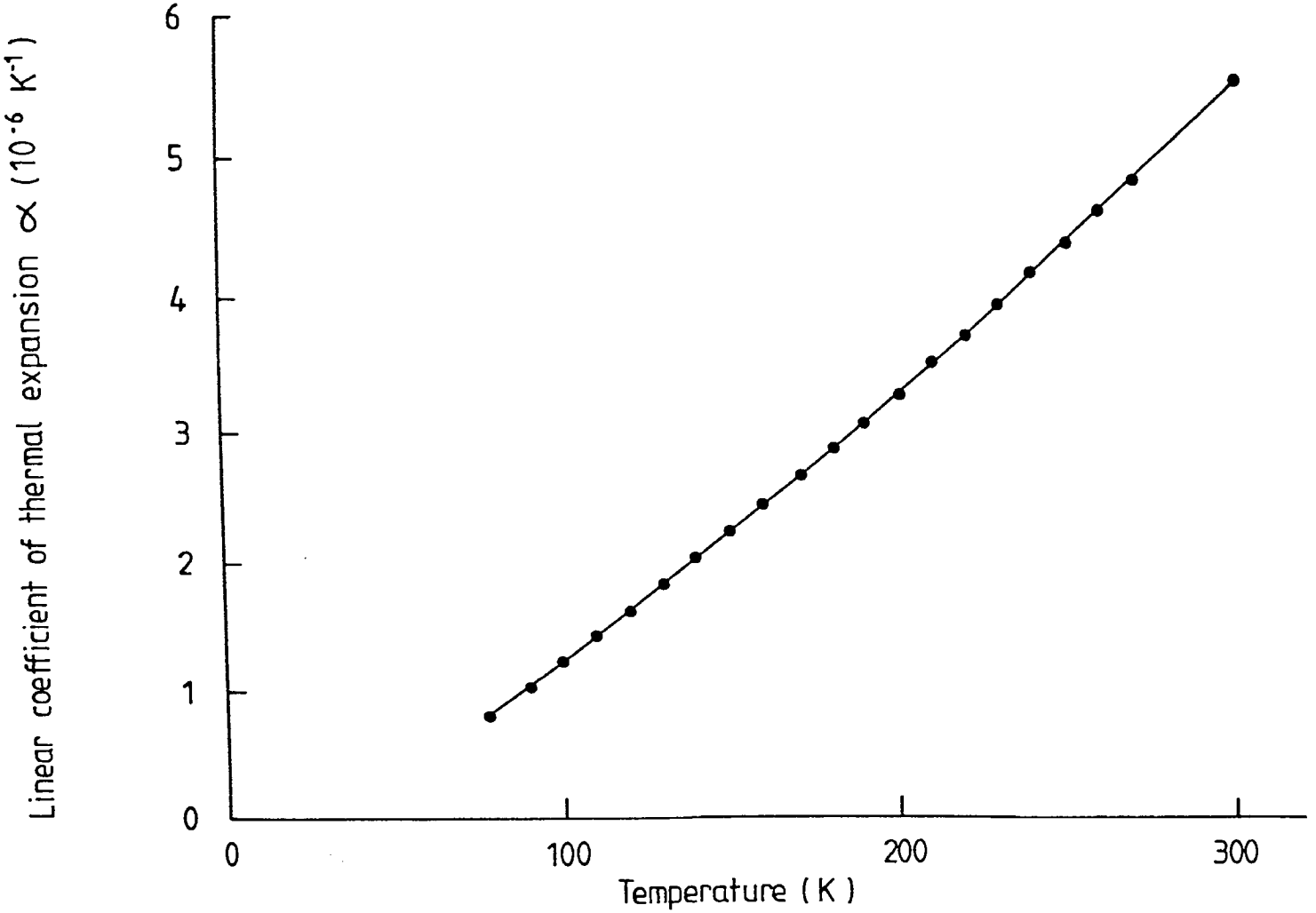

Figure 3.5 Linear coefficients of thermal expansion for $MgAl_2O_4$ as a function of temperature.

CHAPTER 4

RESULTS FOR $ZnFe_2O_4$ SPINEL

4.1 Preparation of $ZnFe_2O_4$

Zinc ferrite spinel can be synthesized by two methods, the mixed oxide method and the mixed nitrate method (the wet method).

The oxide method involves the mixing of appropriate proportions of zince oxide and ferrice oxide according to the following equation

$$ZnO + Fe_2O_3 \rightarrow ZnFe_2O_4$$

As with the preparation of $MgAl_2O_4$ spinel, these oxides were mixed by a mechanical mixer and then compressed into pellets in a hydraulic press under seven tons. The pressed pellets were fired in an oxygen atmosphere several times at temperatures of 1050 K and 1450 K until a zinc ferrite spinel phase was obtained. An oxygen atmosphere was used to eliminate any effect from the dissociation of $ZnFe_2O_4$ at temperatures above 1450 K.

On the other hand, the wet method involves the mixing of

high purity powders of ferric nitrate ($Fe(NO_3)_3.9H_2O$) and zinc nitrate ($Zn(NO_3)_2.6H_2O$). These were dissolved in the least volume of distilled water necessary and the solution heated slowly to evaporate the water without loss of solute. The mixture of dried metal nitrates was prefired at 850 K until all the nitrogen oxides had been driven off, leaving a residue of mixed metal oxides. This residue, in powder form after crushing, could be compressed and fired as before with the mixed oxide method.

The identification of the samples prepared by the oxide and nitrate methods was carried out with the aid of the X-ray powder method using MoKα radiation. This showed that, the oxide method of preparation for $ZnFe_2O_4$ spinel although more convenient, was subject to the presence of small amounts of the constituent oxides. Moreover, it was found that these impurities were not removed when the pellets were reground and pressed again between firings nor by refiring the pellets for another twenty four hours at 1450 K. From these considerations, it seemed desirable to achieve the fine scale mixture by the nitrate method as this did not lead to detectable unreacted constituent oxides after firing.

In the case of the mixed nitrate method, mixing of the solutions means that the ions mix on an atomic scale.

This is most probably the reason why the spinel phase only is found in the final product by the nitrate method. Therefore, brownish black zinc ferrite spinel ($ZnFe_2O_4$) obtained by the nitrate method (see Table 4.1) was used for lattice parameter measurements.

4.2 Choice of X-ray radiation

In the case of $ZnFe_2O_4$ spinel, CuKα radiation cannot be used because of the presence of the iron (Fe) in $ZnFe_2O_4$ which causes a fluorescence effect. To reduce the fluorescence effect, Zr and Mn filters were placed after the sample holder, but it was still impossible to detect any diffraction lines of $ZnFe_2O_4$ spinel except for one or two faint lines. Therefore, MoKα radiation was chosen for the measurement of $ZnFe_2O_4$ lattice parameters. With this radiation, the Xenon proportional counter which was used with CuKα radiation was not suitable and was replaced by a (NaI(Tℓ) scintillation counter.

4.3 Choice of internal standard

The MoKα radiation has a very short wavelength, therefore, there was no other choice but to use the diffraction lines for $ZnFe_2O_4$ within the low angle range. In this

Index (hkl)	Interplanar distance d/A°	Relative intensity I/Imax	Approximate angular position in 2θ°
111	4.87	20-30	8.35
220	2.98	40	13.67
311	2.54	100	16.05
222	2.44	Faint	16.71
400	2.10	40	19.45
422	1.72	40	23.80
511 (333)	1.62	70	25.29
440	1.49	80	27.54
620	1.33	10-20	30.93
533	1.29	40	31.91
622	1.27	Faint	32.43
642	1.13	30	36.58
731 (553)	1.10	50	37.62
800	1.06	30	39.09
751 (555)	0.97	40	42.89
931	0.89	20	46.97
771	0.85	30	49.32
773	0.82	10-20	51.25
(1022) (666)	0.81	10-20	51.93

Table 4.1

X-ray data for $ZnFe_2O_4$ spinel used to check against the A.S.T.M. Index

range, the lines are close to each other and the choice of the internal standard was difficult as the lines from both the $ZnFe_2O_4$ spinel and the internal standard tend to overlap.

Si and Al are the only standards which are similar to the $ZnFe_2O_4$ spinel and have one line each suitable for line position corrections. In the case of Si, the thermal expansion at low temperature is very small and hence difficult to detect in the low angle range. Therefore, Al was chosen as the standard in this case. By experiment it was found that a mixture of 50% of Al with 50% of $ZnFe_2O_4$ gave the best diffraction line definition for lattice parameter measurements.

An important problem which had to be resolved was that only Bandyopadhyay and Gupta (1978) have measured lattice parameters for Al over the whole temperature range between 89 and 300 K but their measurements differ significantly from those of other workers at room or low temperatures. The measurements of Straumanis and Woodard (1971) only cover the range from 40 to 160 K but are in good agreement with the lattice parameter values reported by Figgins et al (1956) for the range 40 to 125 K. The latter workers also give values for the lattice parameter of Al at 273 and 298.7 K (4.04736 A^o and 4.04968 A^o respectively). Further support for the validity of the earlier

measurements is given by values reported for the linear coefficient of thermal expansion, α,

reported by Strelkov and Novikova (1957) for the temperature range 170 to 300 K. Therefore, in this work, the lattice parameters of Straumanis and Woodard were taken as the standard for the temperature range 40 to 160 K and then, values were calculated for the rest of the temperature range till 300 K using the data of Figgins et al and the values for α given by Strelkov and Novikova (see Table 4.2).

4.4 Correction method

The diffracted intensity distribution for the $ZnFe_2O_4$-Al mixture in the low Bragg angle region is shown in Figure 4.1. The most suitable diffraction lines for the lattice parameter determination of $ZnFe_2O_4$ were (333) and (420). In this region there is only one line from Al namely (220) and this, therefore, was used to correct the measured Bragg angles of $ZnFe_2O_4$.

The measured Bragg angles for the (220) reflexion from the aluminium spectrum, $\theta(220)$, are summarized in column two of Table 4.3 and these were used to calculate the experimental d spacings, and hence the corrections (column three of Table 4.3). These corrections were used

TEMPERATURE (K)	a(A°)	
78.5	4.03286	
90.9	4.03337	
101.9	4.03390	
113.7	4.03454	Straumanis and Woodard (1971)
125.2	4.03524	
137.0	4.03601	
148.9	4.03682	
160.8	4.03768	
171.3	4.03849	
182.1	4.03935	
191.8	4.04011	
201.3	4.04089	
212.0	4.04178	
221.4	4.04257	calculated as described in the text
231.3	4.04342	
240.1	4.04419	
248.8	4.04496	
256.2	4.04563	
269.4	4.04682	
273.0	4.04736	← Figgins et al (1956)
276.2	4.04744	calculated as above
288.5	4.04859	
298.7	4.04968	← Figgins et al (1956)
300.0	4.04969	← calculated as above

Table 4.2

Lattice parameters for aluminium

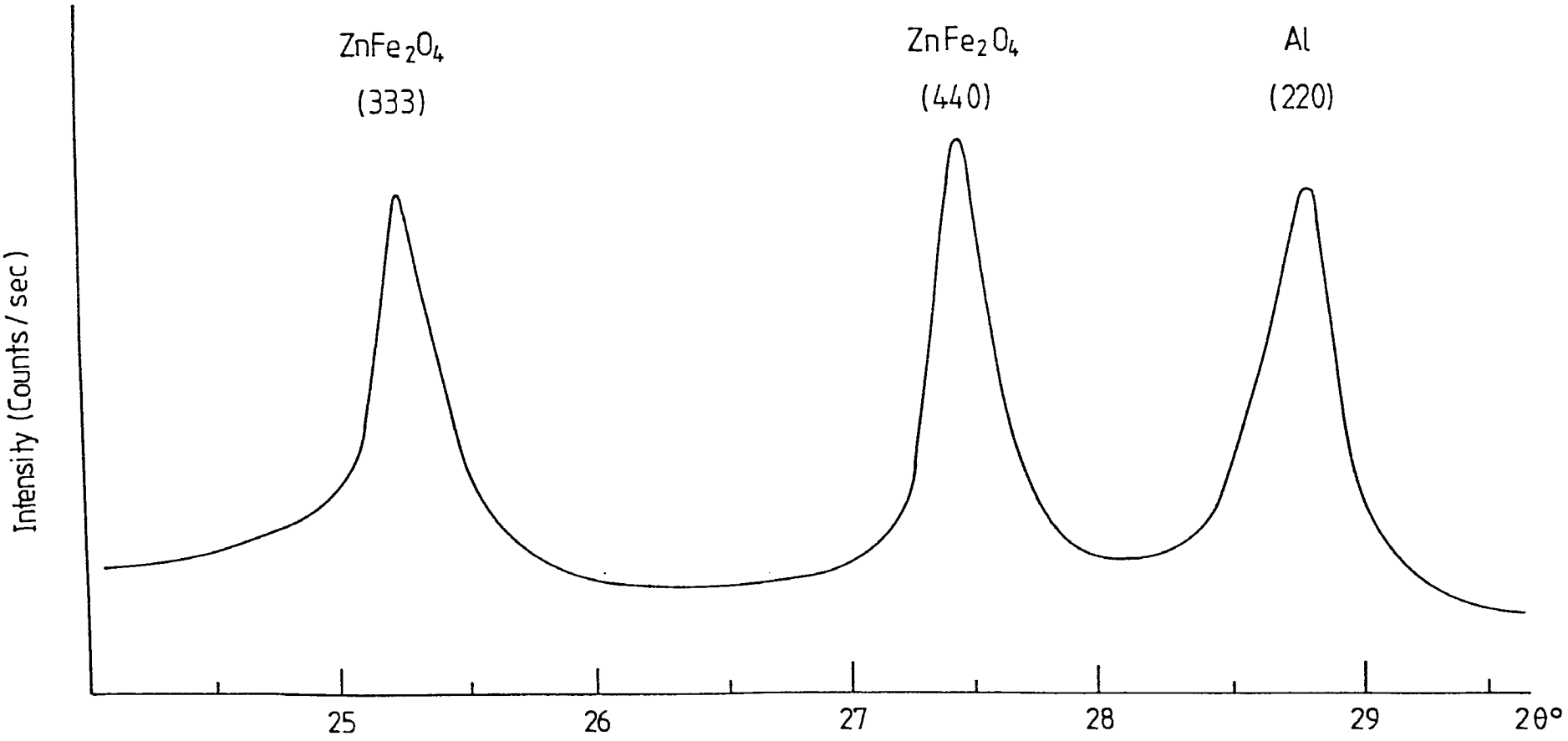

Figure 4.1 The diffracted intensity distribution for the zinc ferrite – aluminium mixture in the low Bragg angle region.

TEMPERATURE (K)	$\theta^{\circ}(220)$	$\Delta\theta^{\circ} \times 10^{-4}$
78.5	14.3888	2.40
90.9	14.3863	2.50
101.9	14.3838	2.61
113.7	14.3813	2.63
125.2	14.3800	2.41
137.0	14.3763	2.55
148.9	14.3738	2.50
160.8	14.3700	2.61
171.3	14.3675	2.53
182.1	14.3638	2.62
191.8	14.3625	2.39
201.3	14.3588	2.53
212.0	14.3550	2.62
221.4	14.3525	2.56
231.3	14.3500	2.47
240.1	14.3463	2.61
248.8	14.3450	2.36
256.2	14.3413	2.57
269.4	14.3375	2.49
276.2	14.3350	2.52
288.5	14.3300	2.68
300.0	14.3275	2.43

Table 4.3

Measured Bragg angles for the (220) line of aluminium with the line position corrections

to correct the Bragg angles of the $ZnFe_2O_4$ lines (333) and (440).

4.5 Determination of lattice parameters as a function of temperature

The measured Bragg angles for the (333) and (440) diffraction lines from $ZnFe_2O_4$ over the temperature range 78.5 to 300.0 K are presented in Table 4.4. These values were corrected and used with the wavelength of $MoK\alpha_1$ radiation (0.7093 A^o) to calculate corresponding lattice parameters $a_{corrected}(333)$ and $a_{corrected}(440)$, as shown in columns two and three of Table 4.5. The average of these lattice parameters (a_{ave}) are presented in column four. Column five gives the smoothed values (a_{smooth}) which result from fitting by a polynomial equation of the third degree in temperature through the average lattice parameters (Figure 4.2). The constant coefficients for best fit are

$$a_0 = 8.4140 \pm 0.0001 \ (A^o)$$

$$a_1 = 0.321 \times 10^{-4} (A^o)$$

$$a_2 = -0.164 \times 10^{-7} \ (A^o)$$

$$a_3 = 0.119 \times 10^{-9} \ (A^o)$$

The root mean square deviation of the smoothed values of lattice parameters from the experimental values was found

TEMPERATURE (K)	θ(333)	θ(440)
78.5	12.6338	13.7750
90.9	12.6325	13.7750
101.9	12.6325	13.7738
113.7	12.6313	13.7738
125.2	12.6313	13.7725
137.0	12.6300	13.7725
148.9	12.6300	13.7713
160.8	12.6288	13.7713
171.3	12.6288	13.7700
182.1	12.6275	13.7688
191.8	12.6288	13.7700
201.3	12.6275	13.7675
212.0	12.6263	13.7675
221.4	12.6263	13.7663
231.3	12.6250	13.7663
240.1	12.6238	13.7650
248.8	12.6250	13.7650
256.2	12.6225	13.7638
269.4	12.6225	13.7625
276.2	12.6213	13.7625
288.5	12.6200	13.7600
300.0	12.6200	13.7600

Table 4.4

Measured Bragg angles for the (333) and (440) line positions of $ZnFe_2O_4$

TEMPERATURE (K)	a_{corr}(333) (A°)	a_{corr}(440) (A°)	a_{ave} (A°)	a_{smooth} (A°)
78.5	8.41652	8.41730	8.41691	8.41648
90.9	8.41695	8.41696	8.41696	8.41687
101.9	8.41655	8.41733	8.41694	8.41723
113.7	8.41724	8.41725	8.41725	8.41761
125.2	8.41813	8.41872	8.41843	8.41800
137.0	8.41842	8.41825	8.41834	8.41840
148.9	8.41860	8.41921	8.41891	8.41881
160.8	8.41901	8.41887	8.41894	8.41923
171.3	8.41928	8.41985	8.41957	8.41962
182.1	8.41977	8.412028	8.42003	8.42002
191.8	8.41980	8.42033	8.42007	8.42039
201.3	8.42011	8.42137	8.42074	8.42077
212.0	8.42060	8.42107	8.42084	8.42120
221.4	8.42082	8.42195	8.42139	8.42159
231.3	8.42199	8.42226	8.42213	8.42202
240.1	8.42224	8.42257	8.42241	8.42241
248.8	8.42240	8.42343	8.42292	8.42280
256.2	8.42327	8.42344	8.42336	8.42315
269.4	8.42357	8.42450	8.42404	8.42378
276.2	8.42424	8.42440	8.42432	8.42412
288.5	8.42447	8.42532	8.42490	8.42475
300.0	8.42541	8.42618	8.42580	8.42537

Table 4.5

Lattice parameter results for $ZnFe_2O_4$

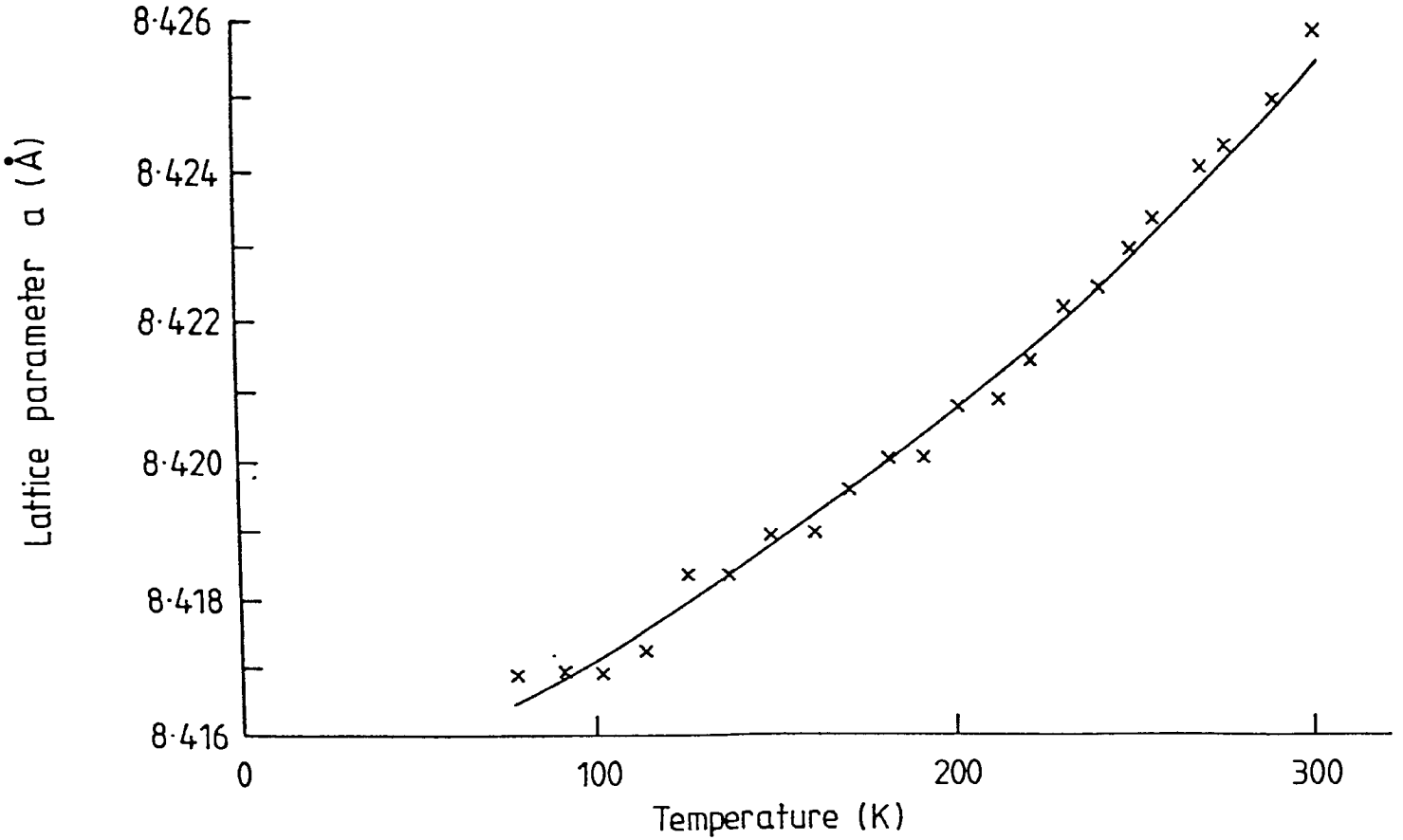

Figure 4.2 The averaged values of lattice parameters for $ZnFe_2O_4$ compared with the smoothed curve as a function of temperature.

to be 0.00025 A^{o} which could be taken as a measure of the precision of the results for the temperature range covered.

4.6 Determination of thermal expansion coefficients as a function of temperature

The linear coefficients of thermal expansion, α, over the temperature range 78.5 to 300.0 K (Table 4.6) were calculated using Equation 2.3 and constants derived from a_1, a_2 and a_3 as follows

$$\alpha_0 = 0.321 \times 10^{-4}/a_T$$

$$\alpha_1 = -0.328 \times 10^{-7}/a_T$$

$$\alpha_2 = 0.357 \times 10^{-9}/a_T$$

As before the volume coefficient of thermal expansion is 3α.

Figure 4.3 shows the temperature dependence of α for $ZnFe_2O_4$, and at 300.0 K, α is found to be $6.46 \times 10^{-6}K^{-1}$.

TEMPERATURE (K)	Linear Coefficients of Thermal Expansion $\alpha(10^{-6}K^{-1})$
78.5	3.77
90.9	3.81
101.9	3.86
113.7	3.92
125.2	3.99
137.0	4.08
148.9	4.17
160.8	4.28
171.3	4.39
182.1	4.51
191.8	4.62
201.3	4.75
212.0	4.89
221.4	5.03
231.3	5.18
240.1	5.32
248.8	5.47
256.2	5.60
269.4	5.84
276.2	5.97
288.5	6.21
300.0	6.46

Table 4.6

Linear coefficients of thermal expansion for $ZnFe_2O_4$

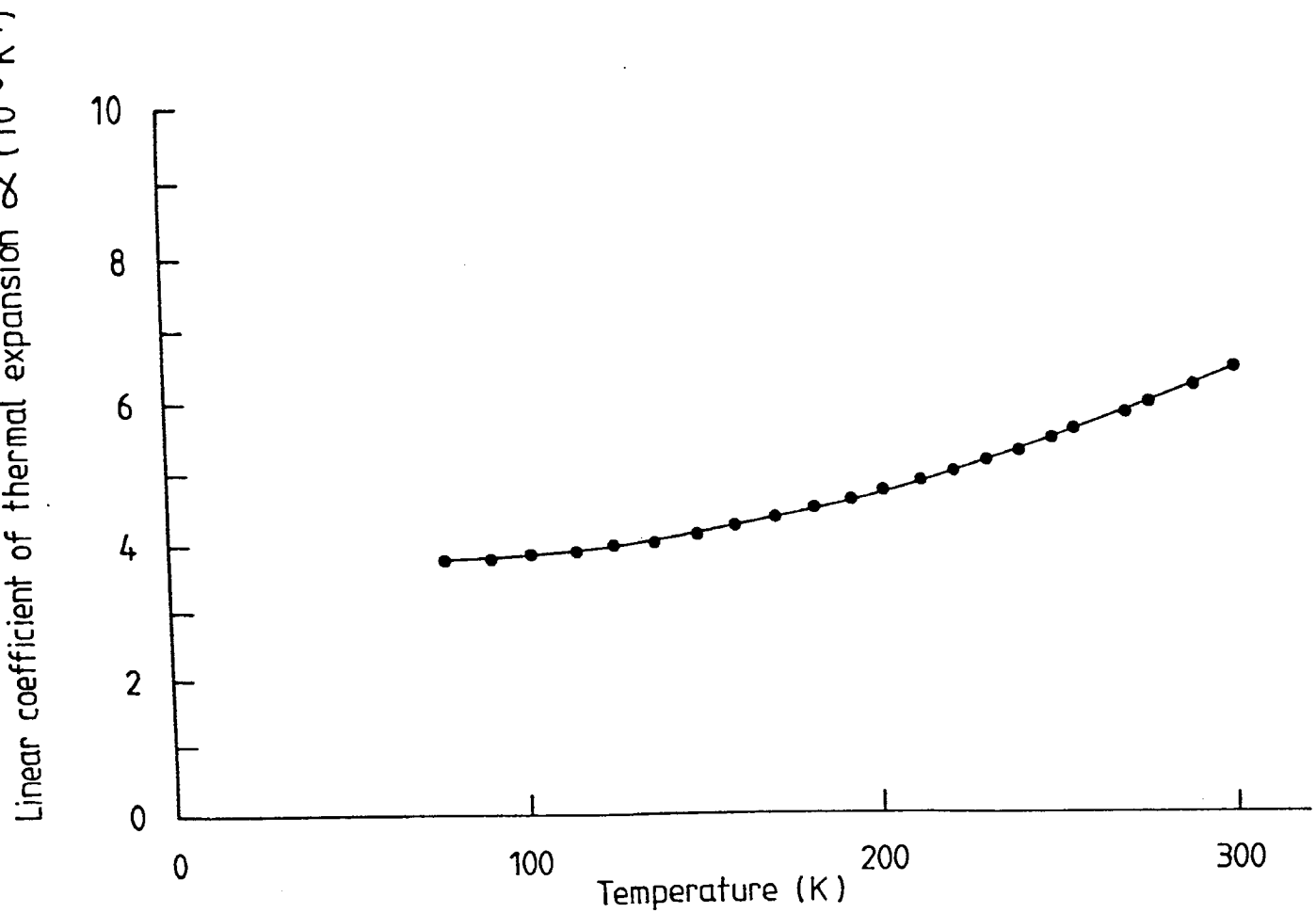

Figure 4.3 Linear coefficients of thermal expansion for $ZnFe_2O_4$ as a function of temperature.

CHAPTER 5

DISCUSSION OF RESULTS

5.1 Comparison with earlier work

Measurements for the lattice parameters of $MgAl_2O_4$ and $ZnFe_2O_4$ have been reported for a range of high temperatures extending down to room temperature and, on the whole, these data are in good agreement. Thus, for example, values in the literature for the room temperature lattice parameter of $MgAl_2O_4$ vary from 8.0799 to 8.0832 A^o (Grimes and Collett 1971; Grimes and Hilleard 1970; Henderson and Taylor 1975; Singh et al 1975; and Suzuki and Kumazawa 1980). The corresponding value reported here, 8.07969 A^o, is slightly lower but should be of higher precision because of the procedures adopted.

Somewhat wider variations exist among the room temperature lattice parameters reported for $ZnFe_2O_4$ as values varying between 8.416 A^o (Hudson and Whitfield 1967), 8.425 A^o (Arkharov and Kuznetsov 1974) and 8.443 A^o (König and Chol 1968; Evans et al 1971) have been found. Such variation may be associated with difficulties in the preparation of this material (see section 4.1). None of these measurements, however, appear to be of comparable

precision to the valve measured in this study (8.42537A^{O}).

It should be emphasized that prior to this work no lattice parameters for $MgAl_2O_4$ and $ZnFe_2O_4$ have been reported below room temperature. Similarly, our data for thermal expansion is new, so that no direct comparison with earlier work is possible. At best we can look for continuity between the earlier results at high temperatures and the low temperature results reported here.

In Figure 5.1, therefore, we show all the available information for the thermal expansion of $MgAl_2O_4$ for the temperature range from 0 to 700 K. Above this temperature range a λ anomaly has been reported by Suzuki and Kumazawa (1980) which is believed may correspond to a change of space group symmetry from $F\bar{4}3m$ at low temperature to Fd3m (See also Mishra and Thomas, 1977).

Figure 5.1 shows that, although the new results seem low at room temperature (300 K) the scatter of the earlier results above this temperature is quite compatible with a continuous smooth curve including the low temperature region. The data of Beals and Cook deviate most from the general trend but generally the agreement is good if allowance is made for possible differences in specimen preparation and stoichiometry and the different techniques employed.

In the case of $ZnFe_2O_4$ the only published thermal expansion

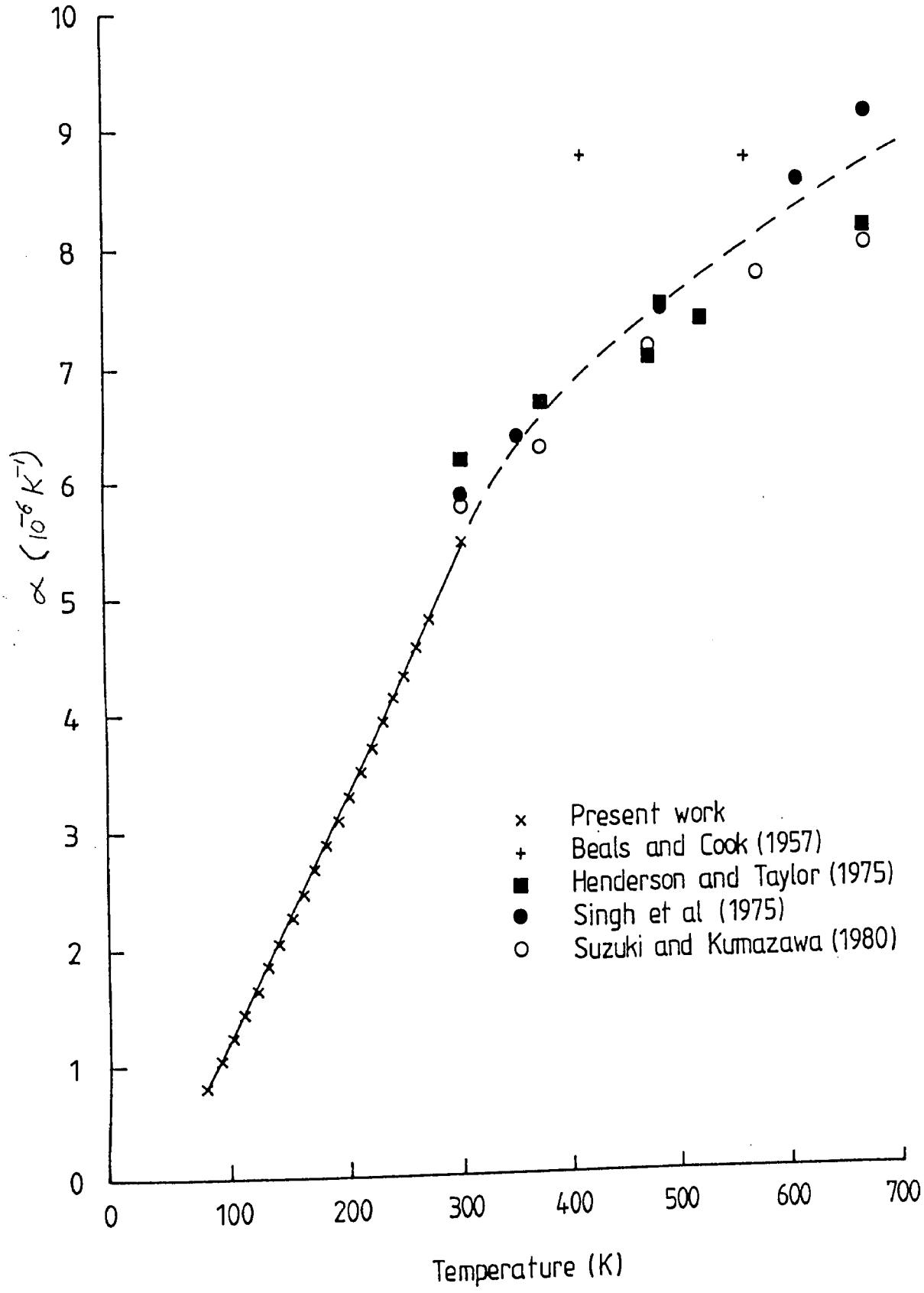

Figure 5.1 Comparison of α for $MgAl_2O_4$ with earlier work.

measurements are those carried out by Weil (1950) who reports mean values for α in four temperature regions. Figure 5.2 shows that the present results are compatible with these measurements although the high temperature results are really too few to be confident about continuity. More generally, however, the agreement between high and low temperature experiments on $MgAl_2O_4$ and $ZnFe_2O_4$ does seem to justify the practice of using specimens formed from a mixture of the spinel compound and an internal standard.

The variation of α with temperature for $MgAl_2O_4$ is apparently well behaved over the temperature range investigated here (see Figure 3.5) and α may be anticipated to tend to zero as the temperature tends to 0 K. $ZnFe_2O_4$, however, appears to behave anomalously in so far that α decreases with decreasing temperature and then becomes almost independent of temperature near 100 K (see Figure 4.3). This result was so surprising that the measurements of lattice parameter over the temperature range 80 to 180 K were repeated and the thermal expansion coefficients recalculated for the corresponding range of temperature. Closely similar results were again obtained and therefore it is concluded that the anomalous behaviour is real and that α does not tend to zero as the temperature tends to 0 K in a simple way in the case of $ZnFe_2O_4$.

The possibility of having such anomalous behaviour among

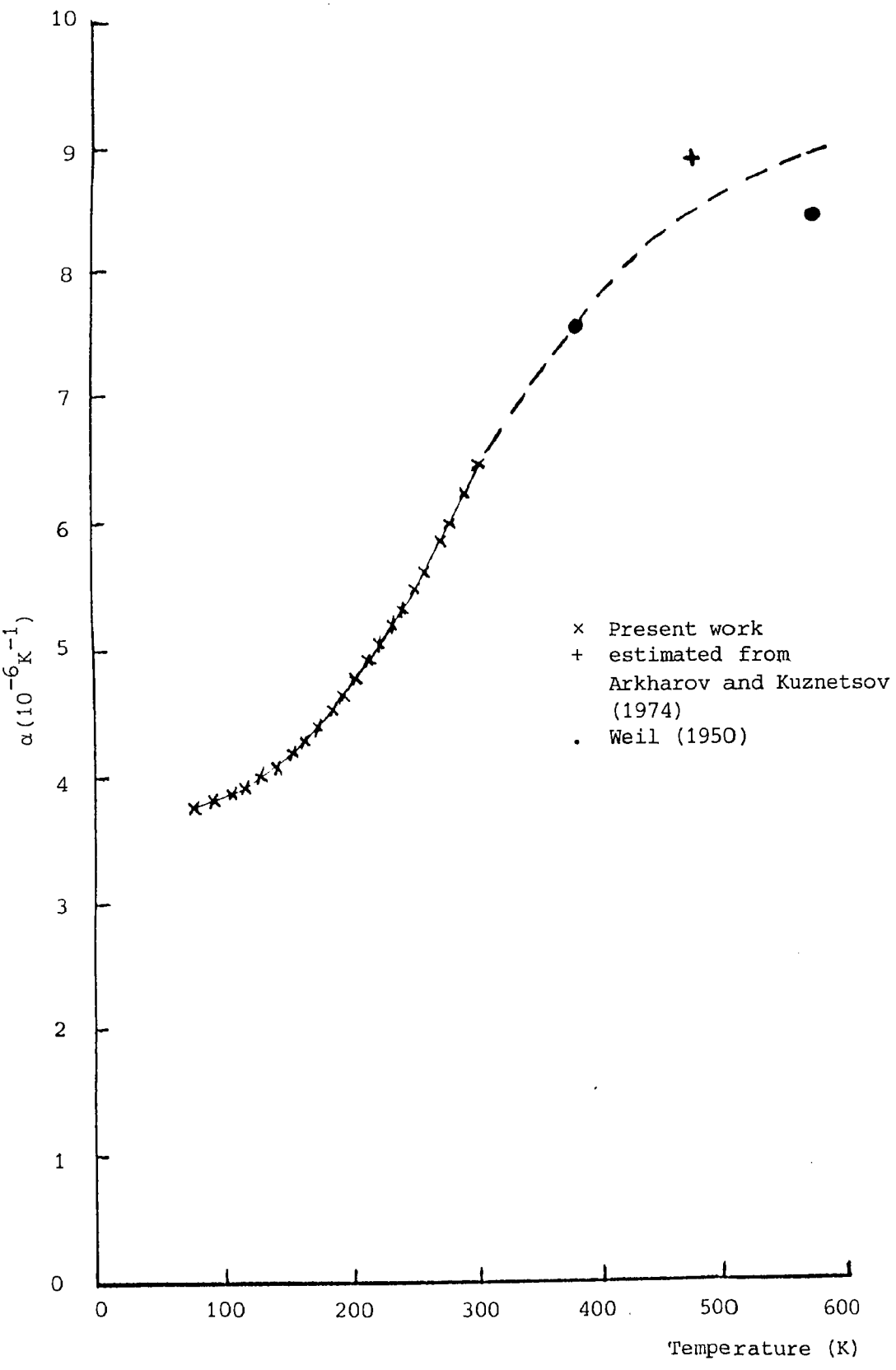

Figure 5.2 Comparison of α for $ZnFe_2O_4$ with earlier work

spinel compounds is not new, for at least two groups of workers have recognized the presence of unusual thermal expansion behaviour in $CdCr_2S_4$ and $CdCr_2Se_4$ with characteristics similar or even more anomalous to that found in this study (Martin et al 1969; Bindloss 1971). The results reported by these workers describe the variation of lattice parameter with temperature for the compounds concerned but a rough calculation for the corresponding variations for α (see Figure 5.3) shows that $CdCr_2S_4$ possesses negative values near 100 K while α for $CdCr_2Se_4$ increases with decreasing temperature below 40 K. The proposed explanation is that in these materials there are displacements taking place internal to the unit cell which are not equivalent to the displacements resulting from hydrostatic pressure. The situation in $ZnFe_2O_4$ is believed to be very similar and indeed there exists a well known specific heat anomaly in this case (see Figure 5.4) which has been interpreted by Grimes (1974) as arising from off-centre displacements of octahedrally coordinated iron. As mentioned previously (see section 1.4.1) the mechanism for such displacements is believed to be associated with the local potential conditions.

In the metallic spinels, the local potential conditions have been shown to be different from other spinel compounds (see section 1.4.3). Some of these materials appear to belong to the class of strong superconductors with high

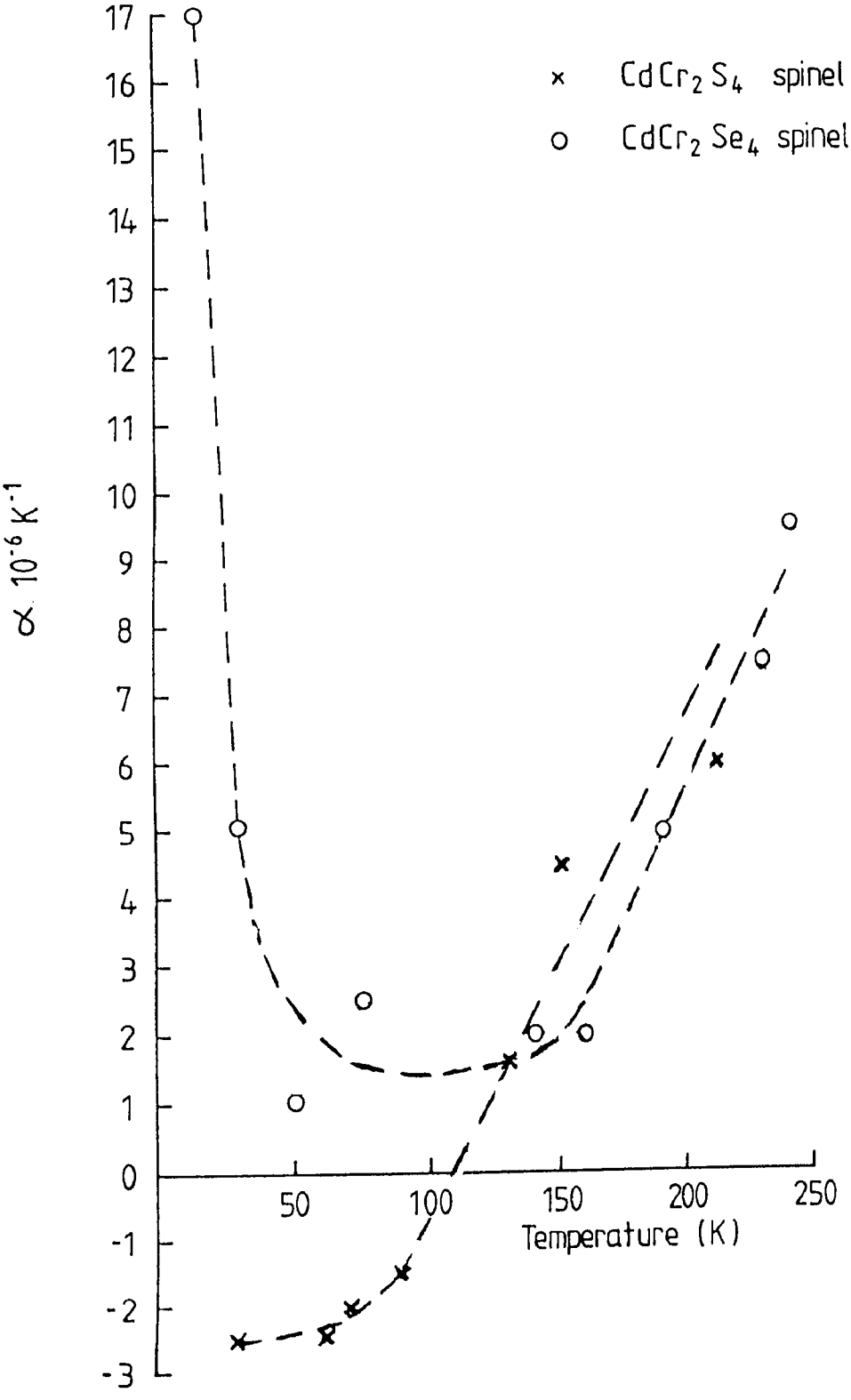

Figure 5.3 Rough estimation of thermal expansion coefficients for $CdCr_2Se_4$ and $CdCr_2S_4$ spinels calculated from lattice parameter measurements reported by Martin et al (1969)

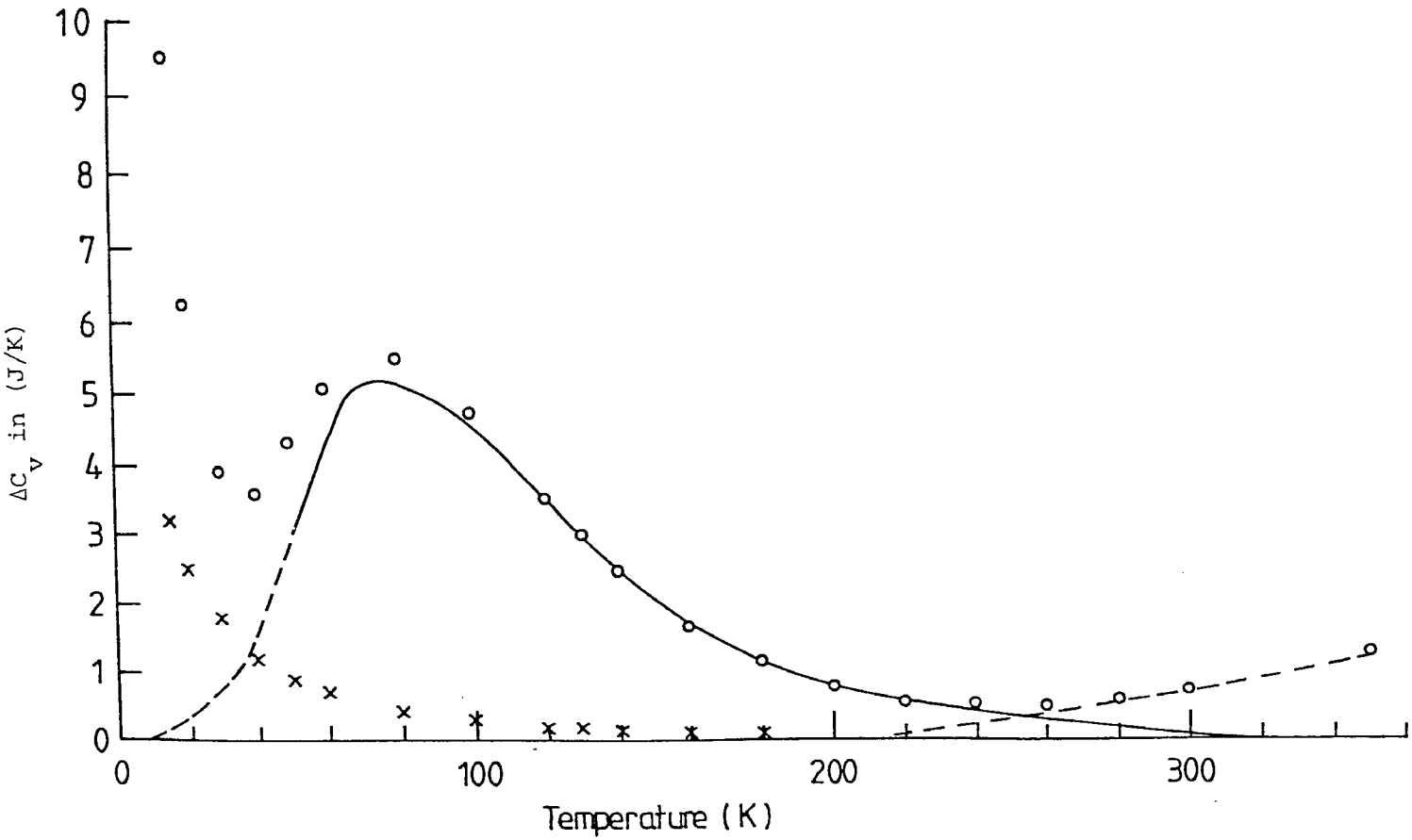

Figure 5.4 ΔC_v as a function of temperature fro $ZnFe_2O_4$. The solid curve is the anomaly arising from the transitions of the Fe^{3+} ion within the octahedral 'hole'. Other contributions are indicated as follows: X,C_m according to Tachiki and Yosida (1957), - - - -, contribution from anharmonic terms (after Grimes, 1974)

transition temperature (Dawes , 1975; Siripairoje 1978). Therefore, it is useful to compare the behaviour of one of these materials ($LiTi_2O_4$) with the other spinel compounds.

Table 5.1 summarizes experimental data for the thermal expansion coefficients of $LiTi_2O_4$ kindly made available by Dr R W Cheary (unpublished work). The temperature dependence of α is shown in Figure 5.5. This variation is reasonably consistent with the value of 15.6 $(10^{-6}K^{-1})$, reported by Roy et al (1977) for the temperature range in the neighbourhood of 660 K.

5.2 The Grüneisen parameter γ

As discussed previously it can be shown that for a quasi harmonic cubic crystal the ratio $\gamma = \beta V/\chi_T C_V$ should be a constant independent of temperature. Therefore, the temperature variation of γ has been used as a relative measure of anharmonicity.

In calculating γ for $MgAl_2O_4$ and $ZnFe_2O_4$ spinels, the present data for thermal expansion have been used in association with the corresponding molar volume calculated according to the following equation $V = (a^3 \times \text{Av.No.})/8$ (see Tables 5.2 and 5.3). The molar heat capacities for these spinels were reported by Grimes (1972c and 1974) and

TEMPERATURE (K)	Linear Coefficient of Thermal Expansion $\alpha(10^{-6}K^{-1})$
80	1.40
90	1.44
100	1.63
110	2.45
120	3.41
130	4.39
140	5.38
150	6.13
160	6.24
170	6.24
180	6.61
190	6.72
200	6.81
210	7.38
220	7.78
230	7.79
240	7.99
250	8.17
260	8.10
270	7.91
280	8.10
290	8.30
300	8.50

Table 5.1

Linear coefficients of thermal expansion for $LiTi_2O_4$

(after Cheary)

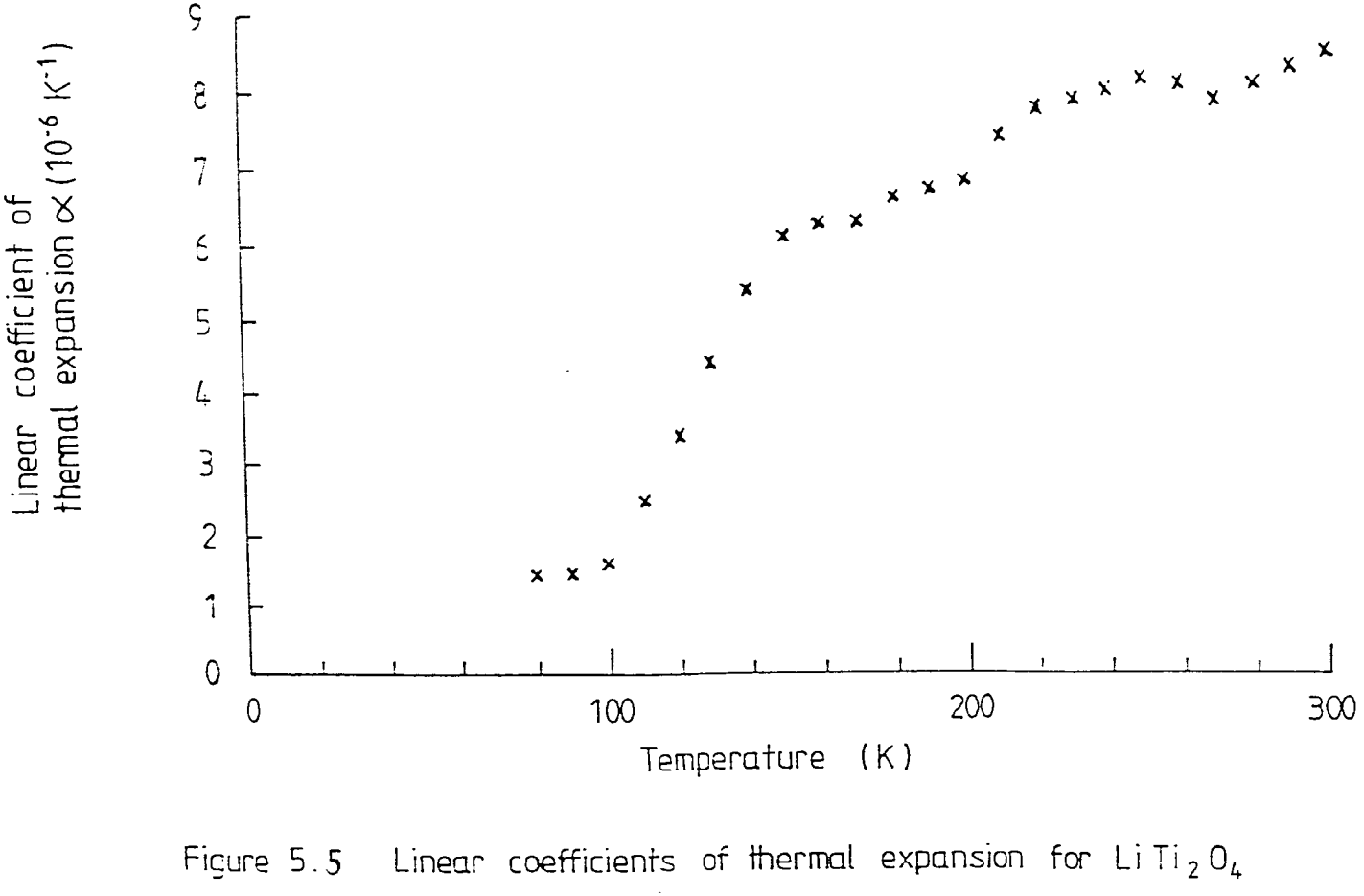

Figure 5.5 Linear coefficients of thermal expansion for $LiTi_2O_4$ (after Cheary)

TEMPERATURE (K)	$V(10^{-6}m^3)$	C_V (J/K)
77.5	39.6290	12.32
89.6	39.6303	17.54
99.6	39.6317	22.08
110.3	39.6334	27.80
120.0	39.6352	33.01
130.0	39.6373	38.72
140.0	39.6395	44.43
150.0	39.6421	50.15
160.0	39.6449	55.86
171.1	39.6483	61.94
180.9	39.6516	67.28
189.8	39.6546	71.85
199.8	39.6585	76.97
210.3	39.6627	81.85
220.1	39.6669	86.40
230.3	39.6716	90.67
240.0	39.6762	94.73
250.0	39.6813	98.49
259.6	39.6863	102.11
270.1	39.6922	105.64
300.1	39.7106	114.91

Table 5.2

The molar volume data and molar heat capacities (Grimes, 1972c) for $MgAl_2O_4$

TEMPERATURE (K)	$V(10^{-6}m^3)$	C_V (J/K)
78.5	44.8864	29.35
90.9	44.8926	38.85
101.9	44.8984	46.82
113.7	44.9044	55.39
125.2	44.9107	63.59
137.0	44.9171	71.62
148.9	44.9236	79.11
160.8	44.9304	86.37
171.3	44.9366	92.03
182.1	44.9430	97.69
191.8	44.9489	102.25
201.3	44.9550	106.62
212.0	44.9619	110.93
221.4	44.9682	114.63
231.3	44.9751	118.04
240.1	44.9813	121.07
248.8	44.9875	123.65
256.2	44.9932	125.84
269.4	45.0033	129.34
276.2	45.0087	131.06
288.5	45.0188	133.90
300.0	45.0287	136.43

Table 5.3

The molar volume data and molar heat capacities (Grimes, 1974) for $ZnFe_2O_4$

this data also is presented in the above tables. Some values for the elastic constants of these materials are summarised in Table 5.4.

The Grüneisen parameters calculated from these data are presented in Tables 5.5 and 5.6 while Table 5.7 presents Grüneisen parameters for $LiTi_2O_4$ reported by Cheary (unpublished work) using data for molar heat capacities from Siripairoje (1978). Figures 5.6, 5.7 and 5.8 show the variation of γ with temperature for the above spinels.

The elastic constants used to evaluate γ for $MgAl_2O_4$ were the values reported at room temperature by Chang and Barsch (1973). However, Pointon and Taylor (1968) have reported that these values increase with decreasing temperature being about 7% higher at 4.2 K and if this is taken into account the graph of the variation of γ (Figure 5.6) will be slightly steeper between 80 and 150 K.

The only published values of γ for spinel compounds are those for $MgAl_2O_4$, where a calculated value of 1.41 (for $T > \theta_o$) has been reported by Chang and Barsch (1973) while Suzuki and Kumazawa give 1.13 at room temperature. The agreement with the present results is therefore satisfactory for we find 1.11 at room temperature and, by extrapolation, a value above 1.4 near θ_o(863 K).

In the case of $ZnFe_2O_4$, the calculation of γ is complicated

by factors arising from the crystallographic structural anomaly previously described (see section 5.1). For example, if full experimental values for C_v are used then this includes a contribution from the Schottky anomaly at 72 K. Therefore Grimes' (1974) theoretical estimates for the lattice vibrational contribution to C_v were used. Similarly because of similarities between $ZnFe_2O_4$ and $ZnCr_2O_4$ it seems likely that elastic relaxations occur with decreasing temperature (Kino and Lüthi, 1971; Kino et al, 1972) and strictly this also should be taken into account. The effect might be to produce a somewhat less steep variation of γ at low temperatures. However, the effect of this possibility is likely to be small and has therefore been neglected.

	T = room temperature					T = 4.2 K				
	C_{11}	C_{12}	C_{44}	$1/\chi$	Ref.	C_{11}	C_{12}	C_{44}	$1/\chi$	Ref.
$MgAl_2O_4$	2.808	1.532	1.5468	1.957	Chang and Barsch (1973)	2.99	1.65	1.65	2.097	Pointon and Taylor (1968)
	2.79	1.53	1.53	1.95	Lewis (1966)					
$ZnFe_2O_4$	2.6500	1.570	1.3500	1.930	Grimes (1973b)					

Table 5.4 Elastic data for cubic spinel compounds (10^{12} dyn/cm^2)

TEMPERATURE (K)	T/θ_o	γ
77.5	0.09	1.52
89.6	0.10	1.37
99.6	0.12	1.30
110.3	0.13	1.21
120.0	0.14	1.15
130.0	0.15	1.10
140.0	0.16	1.06
150.0	0.17	1.04
160.0	0.19	1.02
171.1	0.20	1.00
180.9	0.21	0.99
189.8	0.22	0.99
199.8	0.23	0.99
210.3	0.24	0.99
220.1	0.26	1.00
230.3	0.27	1.01
240.0	0.28	1.02
250.0	0.29	1.03
259.6	0.30	1.04
270.1	0.31	1.06
300.1	0.35	1.11

Table 5.5

The Grüneisen parameters for $MgAl_2O_4$ as a function of temperature with θ_o = 863 K reported by Suzuki and Kumazawa (1980)

TEMPERATURE (K)	T/θ_o	γ
78.5	0.14	3.34
90.9	0.16	2.55
101.9	0.18	2.14
113.7	0.20	1.84
125.2	0.23	1.63
137.0	0.25	1.48
148.9	0.27	1.37
160.8	0.29	1.29
171.3	0.31	1.24
182.1	0.33	1.20
191.8	0.35	1.18
201.3	0.36	1.16
212.0	0.38	1.15
221.4	0.40	1.14
231.3	0.42	1.14
240.1	0.43	1.14
248.8	0.45	1.15
256.2	0.46	1.16
269.4	0.49	1.18
276.2	0.50	1.19
288.5	0.52	1.21
300.0	0.54	1.23

Table 5.6

The Grüneisen parameters for $ZnFe_2O_4$ as a function of temperature with θ_o = 555 K reported by Grimes (1972b)

TEMPERATURE (K)	T/θ_o	γ
10	0.02	26.08
20	0.03	13.41
30	0.05	3.58
40	0.07	2.13
50	0.08	1.66
60	0.10	1.34
70	0.12	1.12
80	0.13	0.98
90	0.15	0.84
100	0.17	0.81
110	0.18	1.06
120	0.20	1.28
130	0.22	1.46
140	0.23	1.61
150	0.25	1.66
160	0.27	1.54
170	0.28	1.42
180	0.30	1.39
190	0.32	1.32
200	0.33	1.26
210	0.35	1.29
220	0.37	1.31
230	0.38	1.26
240	0.40	1.24
250	0.42	1.24
260	0.43	1.20
270	0.45	1.14
280	0.47	1.14
290	0.48	1.15
300	0.50	1.15

Table 5.7

The Grüneisen parameters for $LiTi_2O_4$ (after Cheary) with θ_o = 599 K (Siripairoje, 1978)

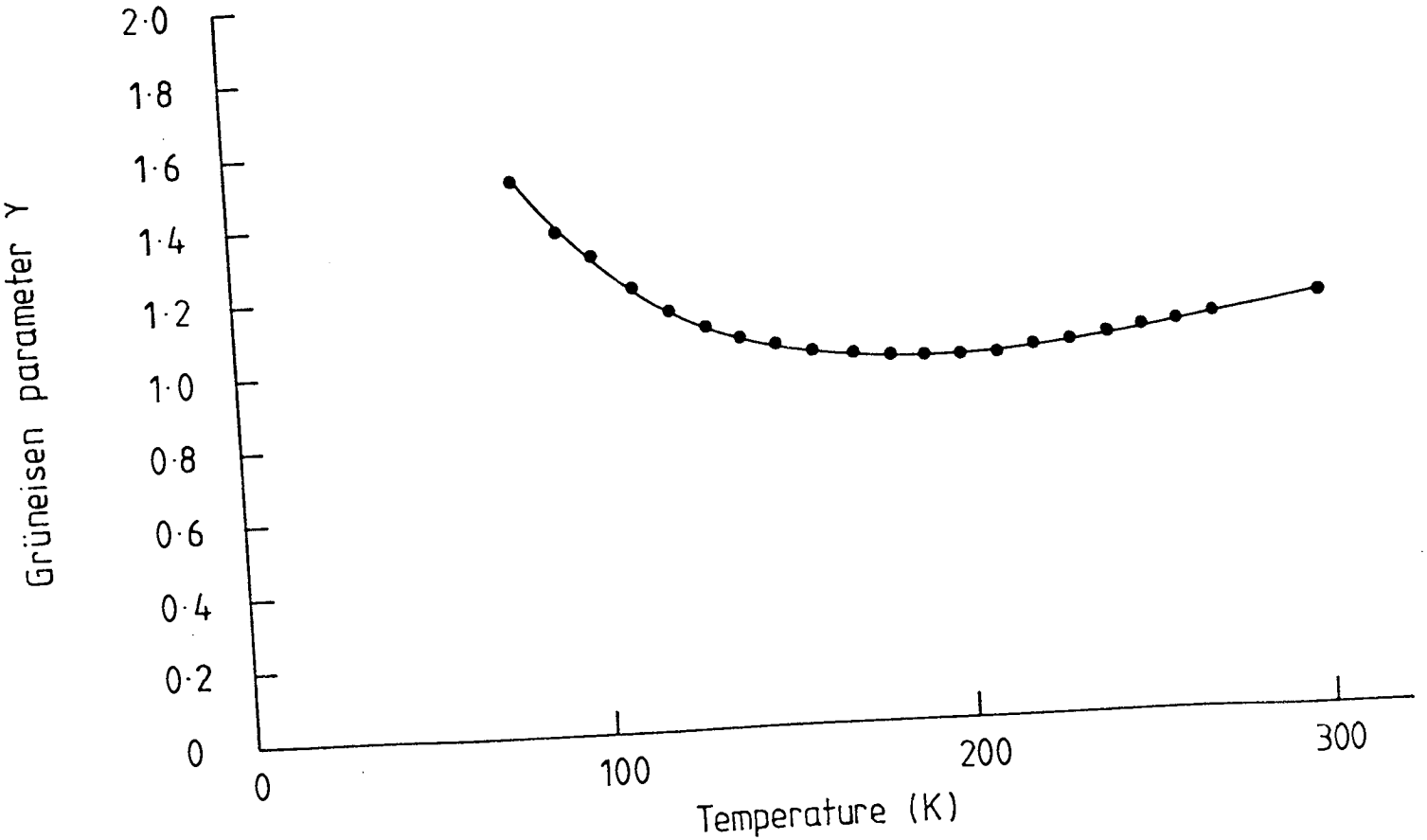

Figure 5.6 Grüneisen parameters of $MgAl_2O_4$ as a function of the temperature

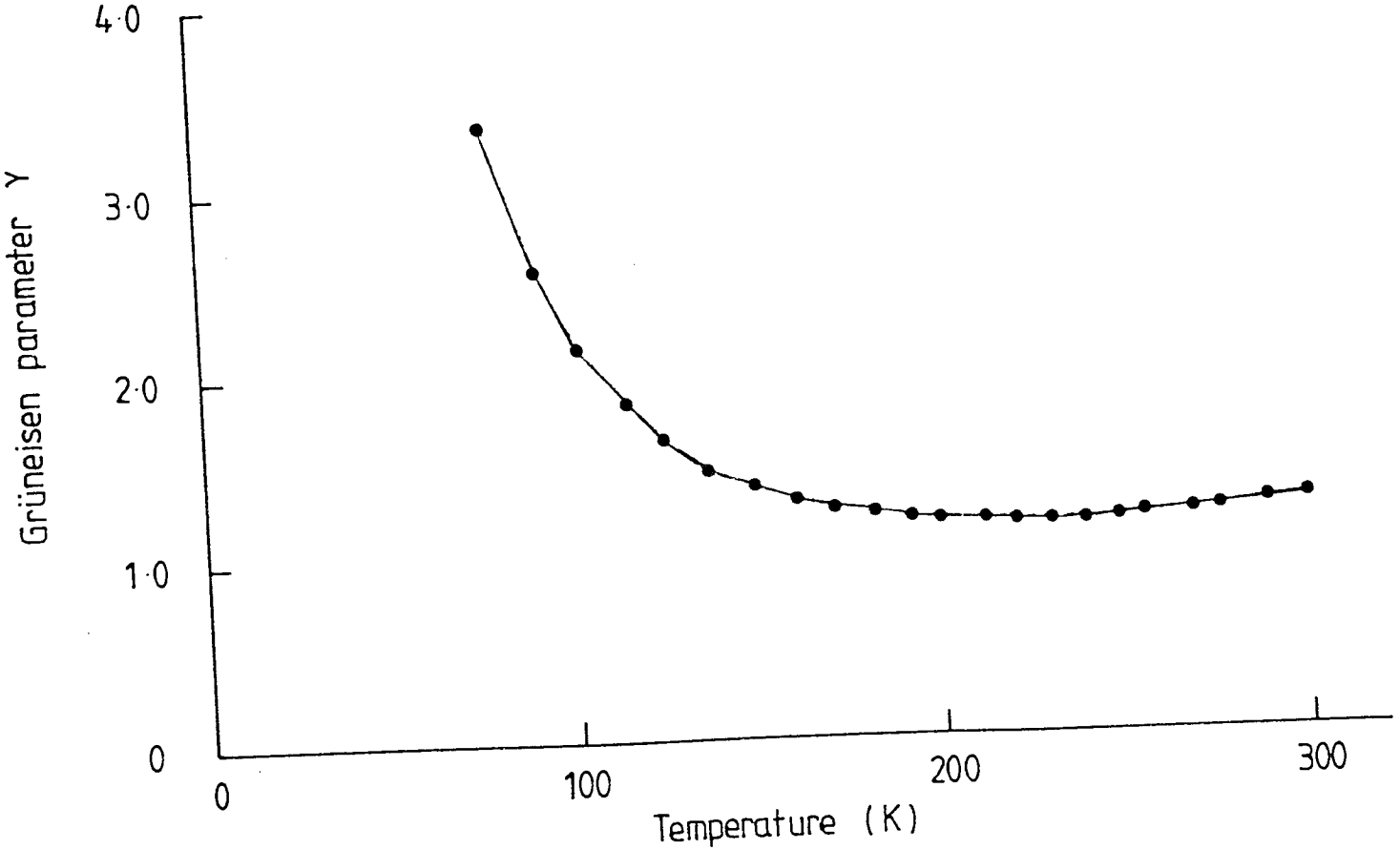

Figure 5.7 Grüneisen parameters of $ZnFe_2O_4$ as a function of temperature

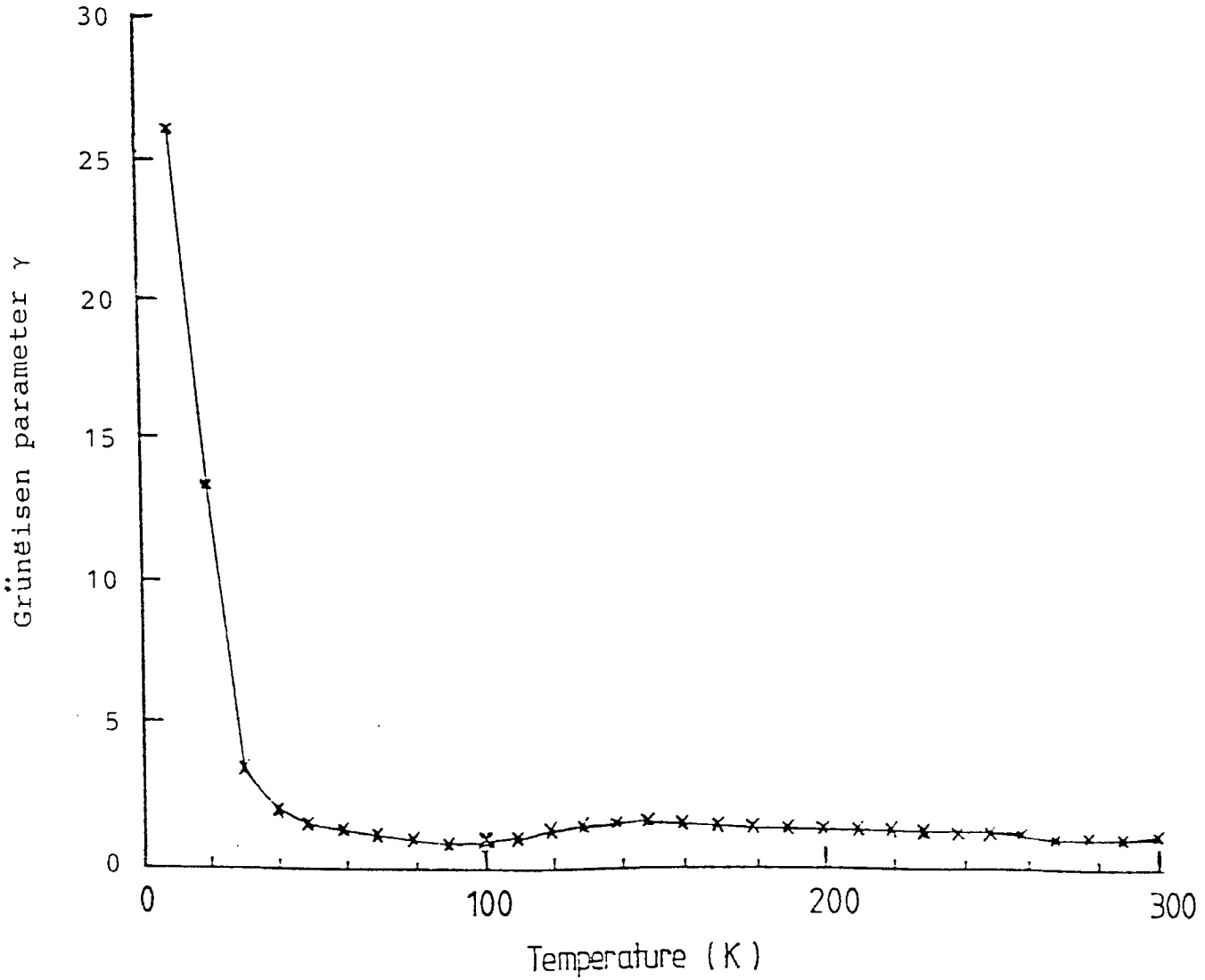

Figure 5.8 Grüneisen parameters of $LiTi_2O_4$ as a function of temperature (after Cheary)

5.3 Discussion

The fact that cubic crystals must by symmetry, possess but one coefficient of thermal expansion makes anomalous behaviour in these materials especially intriguing. Model calculations for various simple crystal structure types have been performed by Barron (1955, 1957) and by Blackman (1958) which indicate that unusual behaviour may be expected in certain circumstances. In particular, it seems that negative volume expansion coefficients are more likely to occur with open structures rather than close packed ones.

On the experimental side the greatest effort seems to have been devoted to investigating compounds crystallizing with the zincblende structure which are well known to show strong anharmonic effects (see section 1.5). Hence it has been shown that many such crystals do indeed possess unusual thermal expansion behaviour including negative coefficients of volume expansion at low temperature. Similarly, γ also can be negative, and the variations of γ with temperature for a range of these crystals are shown in Figure 5.9. According to Smith and White (1975) there is a correlation with the degree of ionicity and this point has been taken up by Gilat (1977) who has argued that when the interatomic forces are mainly central two body interactions, the sign of the thermal expansion coefficients can be negative only

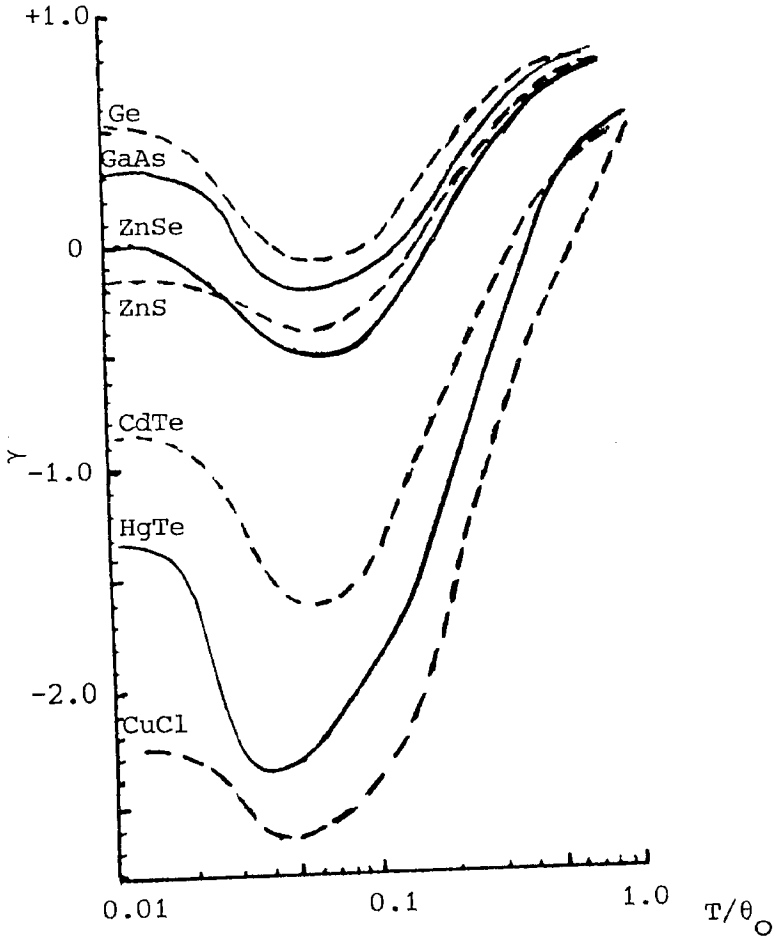

Figure 5.9 $\gamma(T)$ for crystals of zincblende structure (after Barron et al, 1980)

for solids that lack symmetry of inversion.

The importance of this debate for the present work lies in the close relationship between the crystal structures of spinel and diamond. This was first emphasized by Bragg (1915) who imagined each carbon atom in diamond replaced by, for example, one molecule of $MgAl_2O_4$, so that the overall pattern is that of a nearly close packed cubic array of oxygen ions within which the metal ions occupy interstitial positions. In point of fact the analogy with zincblende structure is closer as the space group symmetry $F\bar{4}3m$ is then identical and there is no centre of symmetry.

The similarities between these two systems of chemical compounds are more than merely crystal symmetry. For example, Daniels (1962) has emphasized the very low values for volume expansion among zincblende related materials but the magnitude of β for $MgAl_2O_4$ and $ZnFe_2O_4$ lies in the range 16 to 19.5 ($10^{-6}K^{-1}$) compared with 12 to 22 ($10^{-6}K^{-1}$) for zincblende materials at ordinary temperatures. Similarly, although positive values for β have been found in this study negative thermal expansion does apparently occur, as we have seen, in $CdCr_2S_4$. By contrast, as we show in Appendix A, a simple model for an ionic crystal predicts $\gamma = 13/6$.

Figure 5.10 compares the variation of γ with temperature for the spinel compounds investigated here with the

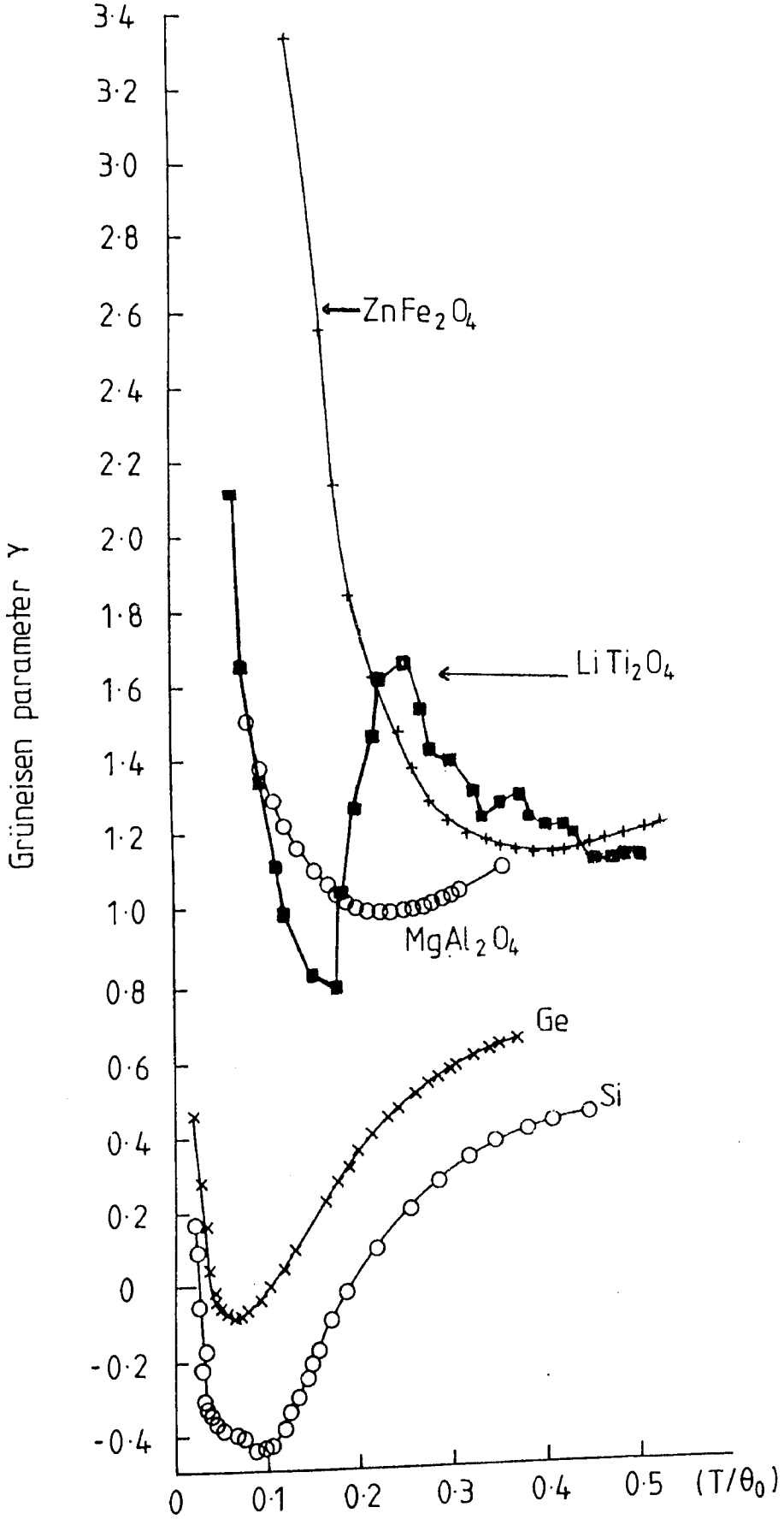

Figure 5.10 Grüneisen parameters as a function of T/θ_0 for Si, Ge, $MgAl_2O_4$, $ZnFe_2O_4$, and $LiTi_2O_4$.

corresponding variation in Si and Ge. We see that there is indeed some similarity which may be connected with the common crystal symmetry and it may be that lower values of γ indicate either a greater degree of anharmonicity or possibly a difference in the repulsive part of the inter-atomic interaction. The mechanism in Si and Ge can not be quite the same since in these cases all atoms within the crystal structure are equal whereas, as we have seen, the spinel materials possess a crystal structure in which one atomic location is anomalous.

This point is emphasized by the difference between the behaviour of $LiTi_2O_4$ and other spinel oxides. If the octahedrally coordinated location in $LiTi_2O_4$ is a site with a flat bottomed potential well then anomalous behaviour at very low temperature should be expected. Indeed, if the full experimental values for C_v for $ZnFe_2O_4$ had been used, i.e., we include the Schottky contribution, then there would be a small dip in the graph of γ in the neighbourhood of $T/\theta_o \cong 0.12$.

CHAPTER 6

CONCLUSIONS AND SUGGESTIONS FOR FURTHER WORK

6.1 Conclusions

In the present investigation of two oxide spinels it has been shown from measurements of thermal expansion that the Grüneisen law relating thermal expansion to heat capacity is not valid over the temperature range 77 to 300 K. In both cases the linear coefficient of thermal expansion is found to be low and there are apparently great similarities to the compounds crystallizing with zincblende structure.

The thermal expansion behaviour of $MgAl_2O_4$ seems to be unexceptional in the low temperature range investigated although a λ anomaly has been reported at much higher temperatures than used in these experiments. There is good continuity between the new low temperature results and published data for the high temperature region.

$ZnFe_2O_4$ is shown to behave differently from $MgAl_2O_4$ in so far that the linear coefficient of thermal expansion becomes independent of temperature at the lowest temperatures investigated and it is clear that this coefficient can not tend to zero as the temperature tends to 0 K as normally

anticipated. By comparison with anomalous expansion behaviour noted by previous workers in $CdCr_2S_4$ and $CdCr_2Se_4$ it is concluded that the behaviour of $ZnFe_2O_4$ is connected with the occurence of internal atomic displacements associated with anharmonic potential conditions at the site occupied by octahedrally coordinated iron.

The local potential conditions at the octahedral site in the metallic spinel $LiTi_2O_4$ are believed to be anharmonic in a different way from insulating $ZnFe_2O_4$ and a comparison of the results obtained by Dr R W Cheary for the Grüneisen parameter with those found here for $MgAl_2O_4$ and $ZnFe_2O_4$ indicates that $LiTi_2O_4$ is certainly not a typical spinel although the linear coefficient of thermal expansion does apparently tend to zero without marked anomalies.

6.2 Suggestions for further work

In calculating the Grüneisen parameter γ for the materials investigated in this thesis it has been necessary to neglect any variation of the elastic constants with temperature as generally speaking very few measurements have been made of these parameters. Clearly, for a more precise study more experimental data for the elastic behaviour is needed.

A considerable amount of experimental data exists

in the literature for the heat capacities of many spinel compounds and this suggests that there is further scope for extending the present studies to other compounds in the spinel series. It would be useful to establish more firmly, for example, the exact relationship between off-centre octahedral site displacements and anomalous expansion behaviour.

Appendix A

THERMAL EXPANSION: GRÜNEISEN'S LAW

To derive a simple relation between thermal expansion and specific heat, it is based on the existence of an asymmetrical potential energy curve for the whole crystal in terms of the separation between atoms. We consider here only the potential energy ϕ between one atom and its neighbour and ignore the problem of coupled interactions. The potential energy curve is shown in Figure 1.6; we transpose it to axes as shown in Figure 1(a) and express ϕ in terms of the displacement r of the atoms from their equilibrium separation a. We assume that at 0 K the energy is zero (ignoring zero-oint energy) and that the addition of thermal energy increases ϕ according to a power law which is used by Tabor, 1969.

$$\phi = Ar + Br^2 + Cr^3 \qquad (1)$$

Since O is the origin where $\frac{\partial \phi}{\partial r} = 0$ we obtain A = O. Then

$$\phi = Br^2 + Cr^3 + ... \qquad (2)$$

If we used only $\phi = Br^2$, the curve would be symmetrical about the ϕ axis and the restoring force for small

(a)

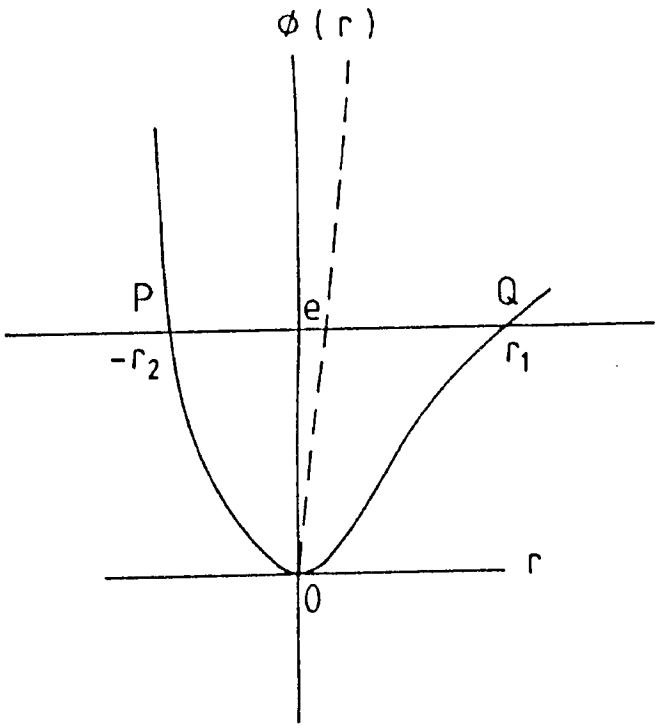

(b)

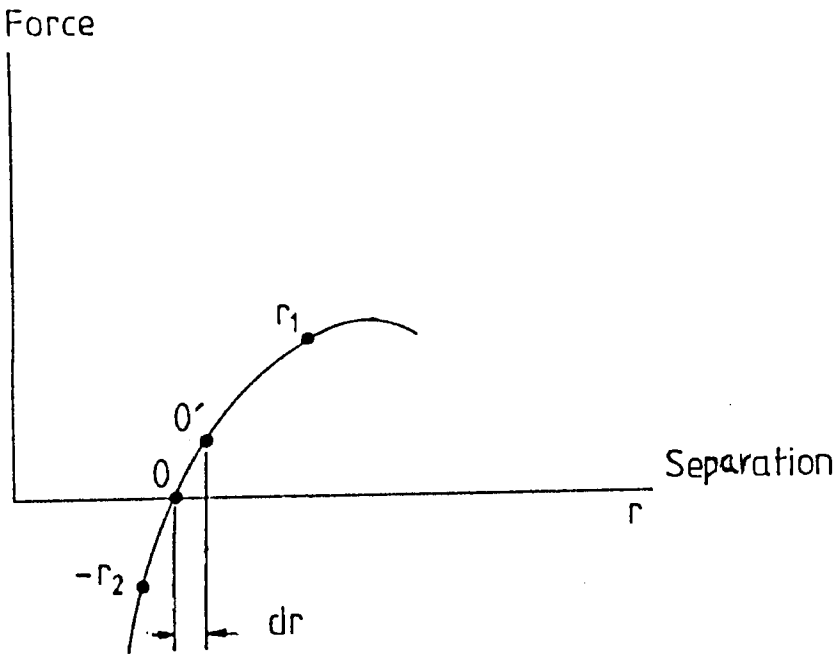

Figure 1 (a) Potential energy transposed to different axes so that the minimum has coordinates 0,0.
(b) Force - separation curve for situation described in (a).
(after Tabor, 1969)

displacements, $-\frac{\partial \phi}{\partial r} = -2Br$, would be proportional to r, so that the atoms would oscillate with simple harmonic motion. We now assume that the cubic term is sufficient to match the real asymmetric potential energy-curve

$$\phi = Br^2 + Cr^3 \qquad (3)$$

At a value of energy ϕ_1, there are two possible values of r, we call them r_1 and $-r_2$

$$\phi_1 = Br_1^2 + Cr_1^3 = Br_2^2 - Cr_2^3$$

$$B(r_1^2 - r_2^2) = -C(r_1^3 + r_2^3) \qquad (4)$$

When adding r_1 and r_2 they can be considered as being almost equal. Equation 4 becomes

$$B(r_1 - r_2) = -Cr^2 \qquad (5)$$

Oscillations between P and Q are not strictly simple harmonic because of the cubic term in r. The mean position, however, is approximately the mid-point of PQ. Its distance e from the ϕ axis is $\frac{1}{2}(r_1 - r_2)$. Hence from Equation (5)

$$e = \frac{-C}{2B} r^2 \qquad (6)$$

The quantity e is the thermal expansion of the lattice when the mean vibrational amplitude is r. Its variation with temperature is

$$\frac{de}{dT} = \frac{-C}{2B} \frac{d}{dT} (r^2) \qquad (7)$$

Now the thermal energy of vibration in one dimension is approximately $\phi = Br^2$ so that the specific heat for a one-dimensional vibration is

$\frac{\partial \phi}{\partial T} = B \frac{d}{dT} (r^2)$.

Since this involves only the vibrational energy, it is the specific heat for constant volume. This makes no assumptions about equipartition of thermal energy so that for this model it holds however far the material may be from the Debye temperature. The specific heat per atom in three dimensions, C_v is three times this, so that

$$C_v = 3B \frac{d}{dT} (r^2) \qquad (8)$$

Hence from equation 7

$$\frac{de}{dT} = \frac{-C}{6B^2} C_v \qquad (9)$$

The coefficient of linear expansion α is given by

$$\alpha = \frac{1}{a} \frac{de}{dT} = \frac{-C}{6B^2} \times \frac{1}{a} C_v \qquad (10)$$

Since a varies little with temperature we see that α is directly proportional to the specific heat at that temperature. The greater the specific heat, the greater the thermal expansion and the greater the effect of the cubic term in augmenting the expansion. This is the main feature of the Grüneisen's treatment.

It is possible to express B and C in terms of other bulk properties of the solid. For example, for a simple cubic array B is equal to Ea/2, where E is Young's modulus. The other parameter chosen by Grüneisen is the rate of change of vibrational frequency with lattice expansion. The natural frequency of vibration ν is proportional to (force constant)$^{\frac{1}{2}}$, i.e. to $\left(\frac{\partial^2 \phi}{\partial r^2}\right)^{\frac{1}{2}}$. Hence

$$\log \nu = \text{constant} + \tfrac{1}{2} \log \frac{\partial^2 \phi}{\partial r^2}$$

$$\frac{d}{dr}(\log \nu) = \tfrac{1}{2}\left(1/\frac{\partial^2 \phi}{\partial r^2}\right) \frac{\partial^3 \phi}{\partial r^3} \qquad (11)$$

From equation (2) we have

$$\frac{\partial^2 \phi}{\partial r^2} = 2B + 6Cr \simeq 2B; \quad \frac{\partial^3 \phi}{\partial r^3} = 6C \qquad (12)$$

Hence $\frac{d}{dr} \log (\nu) = \tfrac{1}{2} \times \frac{6C}{2B} = \frac{3C}{2B}$

But $\frac{d}{dr}(\log a) = \frac{1}{a}$ (13)

Since on the force-displacement curve (Figure 1(b)), the displacement of the equilibrium distance dr is the change in the spacing . Consequently

$$-\frac{d \log \nu}{d \log a} = -\frac{3Ca}{2B} \qquad (14)$$

The Gruneisen constant γ is usually defined in terms of the change of frequency with atomic volume v. Since v is proportional to a^3 , then

$$\gamma = -\frac{d \log \nu}{d \log v} = -\frac{d \log \nu}{3d \log a} = -\frac{Ca}{2B} \qquad (15)$$

Substituting from equation (16)
for $C = -\frac{2B\gamma}{a}$ and $B = \frac{Ea}{2}$ in Equation (10) we obtain

$$\alpha = \frac{2\gamma}{3Ea^3} C_v \qquad (16)$$

For a simple cubic structure $N_o a^3$ is the volume V of a gram-atom and $N_o C_v$ is the specific heat C_v of a gram-atom, hence

$$\alpha = \frac{2\gamma}{3E} \times \frac{C_v}{V} \qquad (17)$$

The coefficient of cubical expansion is 3α so
that $\beta = \frac{2\gamma C_v}{EV}$

A more rigorous model gives

$$\beta = \frac{\gamma C_v}{KV}$$

where K is the bulk modulus.

We see that α is expressed solely in terms of measureable bulk quantities. As a matter of interest we may calculate γ for an ionic solid for which the potential energy between a pair of ions is

$$\phi = -K\left(\frac{1}{r} - \frac{a^8}{9r^9}\right) \qquad (18)$$

$$\ddot{\phi} = \frac{\partial^2\phi}{\partial r^2} = -K\left(\frac{2}{r^3} - \frac{10a^8}{r^{11}}\right) = K\frac{8}{a^3} \text{ at } r = a$$

$$\dddot{\phi} = \frac{\partial^3\phi}{\partial r^3} = -K\left(\frac{-6}{r^4} + \frac{110a^8}{r^{12}}\right) = -K\frac{104}{a^4} \text{ at } r = a$$

From Equations (11) and (13) we see that

$$\gamma = \frac{-\,d \log \nu}{d \log v} = \frac{-\,d \log \nu}{3d \log a} = -\frac{a}{6}\frac{\dddot{\phi}}{\ddot{\phi}} \qquad (19)$$

Consequently for an ionic solid

$$\gamma = +\frac{a}{6} \times \frac{104a^3}{8a^4} = +\frac{13}{6}$$

The above treatment has one basic defect; namely that it treats the solid as though its behaviour were exactly analogous to that of a pair of atoms. By contrast when we consider the behaviour of an assembly of a large number of atoms as in a solid crystal, an entropy factor arises which is not accounted for by the simple treatment. It

may indeed be shown that even if the atomic vibrations were perfectly harmonic, that is if the potential energy curve were perfectly symmetrical, the increase in free energy of the crystal as its temperature is raised would lead to an increase in volume. However, the thermal expansion due to this factor appears to be small compared with that arising from the asymmetric nature of the potential energy curve considered above.

REFERENCES

Arkharov V.I. and Kuznetsov E.N. 'Thermal expansion of zinc ferrite'. Sov. Phys. Dokl. 19, No.3, 142 (1974).

Baltzer P.K., Wajtowicz P.J., Robbins M. and Lopatn E. 'Exchange interactions in ferromagnetic chromium chalcognide spinels'. Phys. Rev. 151, No.2, 367-377 (1966).

Bandyopadhyay J. and Gupta K.G. 'Low temperature lattice parameters of Al and Al-Zn alloys and Grüneisen parameter of Al'. Cryogenic 18, No.1, 54-55 (1978).

Barron T.H.K. 'On the thermal expansion of solids at low temperatures'. Phil. Mag. 46, 720-734 (1955).

Barron T.H.K. 'Grüneisen parameters for the equation of state of solids'. Ann. Phys. (New York), 1, No. 1, 77-90 (1957).

Barron T.H.K., Collins J.G. and White G.K. 'Thermal expansion of solids at low temperatures'. Advances in Physics 29, No.4, 609-730 (1980).

Batchelder D.N. and Simmons R.O. 'Lattice constants and thermal expansivities of silicon and calcium fluoride between 6 and 322 K'. J. Chem. Phys. 41, No.8, 2324-2329 (1964).

Beals R.J. and Cook R.L. 'Directional dilatation of crystal lattices at elevated temperature'. J. Amer. Ceram. Soc. 40, 279-284 (1957).

Bindloss W. 'Anomalous exchangestriction in ferromagnetic pyrite and chromium chalcogenide spinel compounds'. J. Appl. Phys. 42, 1474-1475 (1971).

Blackman M. 'On negative volume expansion coefficients'. Phil. Mag. 3, 831-838 (1958).

Brabers V.A.M. 'Infrared spectra of cubic and tetragonal manganese ferrites'. Phys. Stat. Sol. 33, 563-572 (1969).

Bragg W.H. 'The structure of the spinel group of crystal' Phil. Mag. 30, 305-315 (1915).

Carr R.H., McCammon R.D. and White G.K. 'Thermal expansion of germanium and silicon at low temperatures'. Philos. Mag. 12, 157-163 (1965).

Cervinka L. 'Comparison of lattice vibrations in nickel and manganese - ferrite single crystals'. Czech. J. Phys. B15, No.6, 425-427 (1965).

Change Z.P. and Barsch G.R. 'Pressure dependence of single-crystal elastic constants and anharmonic properties of spinel'. J. of Geophys. Res. 78, No.14, 2418-2433 (1973).

Cheary R.W. 'The application of X-ray diffraction line profile analysis to the study of anti-phase domains in Lithium ferrite'. PhD Thesis, University of Aston in Birmingham (1971).

Daniels W.B. 'The anomalous thermal expansion of germanium, silicon and compounds crystallizing in the zincblende structure'. Report of international conference on the physics semiconductors, 482-489 (1962).

Dash J.G., Johnson D.P. and Visscher W.M. 'Low temperature anharmonicity and the Debye-Waller factor'. Phys. Rev. 168, No.3, 1087-1094 (1968).

Dawes P.P. 'Low temperature anharmonicity in the superconducting spinels' PhD Thesis of Aston University in Birmingham (1975).

Dawes P.P., Grimes N.W. and O'Connor D.A. 'Direct experimental evidence for low termperature anharmonicity'. J. Phys. C: Sol. St. Phys. 7, 17, L387-389 (1974).

Dawson B. and Willis B.T.M. 'Anharmonic vibration and forbidden reflexions in silicon and germanium'. Proc. Roy. Soc. Lond. A. 298, 307-315 (1967).

Dunitz J.D. and Orgel L.E. 'Electronic properties of transition-metal oxides - I' J. Phys. Chem. Solids. 3, 20-29 (1957).

Evans B.J., Hafner S.S. and Weber H.P. 'Electric field gradients at Fe in ZnFe O and CdFe O '. J. Chem. Phys. 55, No.11, 5282-5288 (1971).

Fairweather A., Roberts F.F. and Welch A.J.E. 'Ferrites'. Rep. Prog. Phys. 15, 142-172 (1952).

Figgins B.F., Jones G.O. and Riley D.P. 'The thermal expansion of aluminium at low temperatures as measured by an X-ray diffraction method'. Phil. Mag 1, 747-758 (1956).

Finch G.T., Sinha A.P.B. and Sinha K.P. 'Crystal distortion in ferrite-manganite'. Proc. Roy. Soc. A 242, 28-35 (1958).

Gibbons D.F. 'Thermal expansion of some crystals with the diamond structure'. Phys. Rev. 112, No.1, 136-140 (1958).

Gilat G. 'General qualifications for the sign of thermal expansion coefficients at low temperatures'. Sol. Stat. Commun. 23, 567-570 (1977).

Gomez M., Bowen S.P. and Krumhansl J.A. 'Physical properties of an off-centre impurity in tunnelling approximation. I. Statistics'. Phys. Rev. 153, 1009-1024 (1967).

Gorter E.W. 'Saturation magnetization and crystal chemistry of ferrimagnetic oxides'. Philips. Res. Rep. 9, 295-320 (1954).

Grimes N.W. 'Structural distortions in $MgCr_2O_4$' J. Phys. C:Sol. Stat. Phys. 4, L342-344 (1971).

Grimes N.W. 'Off-centre ions in compounds with spinel structure'. Philos. Mag. 26, 1217-1226 (1972a).

Grimes N.W. 'Self diffusion in compounds with spinel structure'. Philos. Mag. 25, 67-76 (1972b).

Grimes N.W. 'Interpretation of the infrared spectrum of spinels'. Spectrochimica Acta 28A, 2217-2225 (1972c).

Grimes N.W. 'Antiferroelectricity among compounds with spinel structure'. J. Phys. C: Sol. Stat. Phys. 6, L78-79 (1973a).

Grimes N.W. 'Elastic constants for zince ferrite from the infrared spectrum'. Phys. Stat. Sol. b58, L129-132 (1973b).

Grimes N.W. 'On the specific heat of compounds with spinel structure II. Zinc ferrite, a paramagnetic compound with magnetic ion occupying the octahedral site'. Proc. R. Soc. Lond. Ser. A, 338, 223-233 (1974).

Grimes N.W. 'The spinels: versatile materials'. Physics in Technology 6, 22-27 (1975).

Grimes N.W. and Collett A.J. 'Correlation of infrared spectra with structural distortions in the spinel series $Mg(Cr_xAl_{2-x})O_4$' Phys. Stat. Sol., b43, 591-599 (1971).

Grimes N.W. and Hilleard R.J. 'X-ray diffraction studies of the spinel series $Mg(Cr_xAl_{2-x})O_4$ I: lattice parameters and structure'. J. Phys. C.: Sol. Stat. Phys. 3, 866-871 (1970).

Grimes N.W., O'Connor P.J. and Thompson P. 'Comments on the interpretation of the infrared spectrum from $MgAl_2O_4$ spinel'. J. Phys. C: Sol. Stat. Phys. 11, L505-507 (1978).

Grimes N.W., Thompson P. and Kay H.F. 'New symmetry and structure for spinel'. Proc. R. Soc. Lond. A386, 333-345 (1983).

Grüneisen E. "State of a solid body'. NASA (Nat. Aeronaut. Space Admin.) publ.,N. RE 2-18-59 W (translation of Handbuch der Physik) 10, 1-52 (1926).

Hastings J.M.H. and Corless L.M. 'An antiferromagnetic transition in zinc ferrite'. Phys. Rev. 102, No.6, 1460-1463 (1956).

Henderson C.M.B. and Taylor D. 'Thermal expansion by X-ray diffraction: use of specimen holder as internal standard and expansion of MgO (periclase) and $MgAl_2O_4$ (spinel)'. Trans. J. Br. Ceram. Soc. 74, 55-57 (1975).

Hudson A. and Whitfield H.J. 'Electric field gradients in normal spinels'. Molec. Phys. 12, No.2, 165-172 (1967).

Huer A.H. and Mitchell T.E. 'Further discussion on the space group of spinel'. J. Phys. C.: Sol. Stat. Phys. 8, L541-543 (1975).

Hwang L., Huer A.H. and Mitchell T.E. 'On the space group of $MgAl_2O_4$' Phil. Mag. 28, 41-43 (1973).

Keating D.T., Nures A., Batterman B.W. and Hastings J. 'Forbidden (220) neutron reflexion silicon: anharmonicity and the bonding electrons'.

King E.G. 'Heat capacities at low temperatures and entropies at 298.16K of crystalline calcium and magnesium aluminates'. J. Phys. Chem. 59, 218-219 (1955).

Kino Y. and Lüthi B. 'Magnetic and elastic properties of zinc chromite'. Sol. Stat. Comm. 9, 805-808 (1971).

Kino Y., Lüthi B. and Mullen M.E. 'Cooperative Jahn-Teller phase transition in the nickel-zinc-chromite system'. J. Phys. Soc. Japan, 33, 687-697 (1972).

Knapp G.S., Bader S.D., Culbert H.V., Fradin F.Y. and Klippert T.E. 'Heat capacity of V_3X compounds and the relationship between T_c and anharmonicity'. Phys. Rev. B11, 4331-4338 (1975).

Koops, C.G. 'On the dispersion of resistivity and dielectric constant of some semiconductors at audio-frequencies'. Phys. Rev. 83, 121-124 (1951).

König U and Chol G. 'Rontgenbeugungs - und Neutronenbeugungs unter such ungen an ferrite der reihe $Mn_xZn_{1-x}Fe_2O_4$'. J. Appl. Cryst. 1, 124-126 (1968).

Ladany I and Wang C.C. 'Properties of GaP light-emitting diodes grown on spinel substrate'. Sol. Stat. Electronics 17, 573-576 (1974).

Lotgering F.K. 'Paramagnetic susceptibilities of Fe^{2+} and Ni^{2+} ions at tetrahedral or octahedral sites of oxides'. J. Phys. Chem. Solids 23, 1153-1167 (1962).

Lou F.H. and Ballentyne D.W. 'Visible and ultra-violet emission and absorption spectra of $MgAl_2O_4$:Cr'. J. Phys. C.: Proc. Phys. Soc. Ser. 2, 1, 608-613 (1968).

Lyon K.G., Salinger G.L., Swenson C.A. and White G.K. 'Linear thermal expansion measurements on silicon from 6 to 340K' J. Appl. Phys. 48, No.3, 865-868 (1977).

Manasevit H.M. and Forbes D.H. 'Single-crystal silicon on spinel' J. Appl. Phys. 37, No.2, 734-739 (1966).

Martin G.W., Kellogg A.T., White R.L. and White R.M. 'Exchangestriction in $CdCr_2S_4$ and $CdCr_2Se_4$' J. Appl. Phys. 40, No.3, 1015-1016 (1969).

Marumo F., Isobe M., Saito Y., Yagi T. and Akimoto S. 'Electron-density distribution in crystals of γ-Ni_2SiO_4' Acta. Cryst. B30, 1904-1906 (1974).

Matthias B.T. 'New superconducting critical temperatures and field'. I.E.E.-Trans. on. Mag. Mag-11, (2), 154 (1975).

McClure D.S. 'The distribution of transition metal cations in spinel'. J. Phys. Chem. Solids 3, 311-317 (1957).

Mishra R.K. and Thomas G. 'Structural phase transition in the spinel $MgAl_2O_4$' Acta. Cryst. A33, 678 (1977).

Moran T.J. and Luthi B. 'Elastic and Magnetoelastic effects in magnetite'. Phys. Rev. 187, No.2, 710-714 (1969).

Nishikawa S. 'Structure of some crystals of spinel group'. Proc. Tokyo-Math-Phys. Soc. 8, 199-209 (1915).
Peters J. and Standley K.J. 'The dielectric behaviour of magnesium ferrite'. Proc. Phys. Soc. 71, 131-133 (1958).

Pike E.R. and Wilson A.J.C. 'Counter diffractometer - The theory of the use of the centroids of diffraction profiles for high accuracy in the measurement of diffraction angles'. British J. Appl. Phys. 10, 57-68 (1959).

Pointon A.J. and Taylor R.G.F. 'Elastic constants of magnesia, calcia and spinel at 16 GHz and 4.2 K, Nature, 219, 712 (1968).

Polder D. 'Ferrite materials'. Proc. I.E.E., 97 (Part II), 246-256 (1950).

Roberto, J.B., Batterman, B.W. and Keating D.T. 'Forbidden (222) neutron reflection in germanium, anharmonicity in the nuclear motion'. Phys., Stat. Sol. b59, K59-K61 (1973)

Roberto J.B., Batterman B.W. and Keating D.T. 'Diffraction studies of the (222) reflection in Ge and Si: Anharmonicity and the bonding electrons'. Phys. Rev. B9, No.6, 2590-2599 (1974).

Roy, U., Petrov K., Isolovski I. and Peshev P. 'On the structural phase transition and the thermal expansion of spinel lithium titanate'. Phys. Stat. Sol. a44, K25-K27 (1977).

Samuelsen E.J. and Steinsvoll O. 'On the space groupf of spinel'. J. Phys. C.: Sol. Stat. Phys. 8, L427-429 (1975).

Shier J.S. and Taylor R.D. 'Temperature dependent isomer shift and anharmonic binding of Sn^{119} in Nb_3Sn'. Sol. Stat. Commun. 5, 147-149 (1967).

Shier J.S. and Taylor R.D. 'Temperature-dependent isomer shift and anharmonic binding of Sn^{119} in Nb_3Sn from Mossbauer-effect measurements'. Phys. Rev. 174, 346-350 (1968).

Singh H.P., Simmons G. and McFarlin P.F. 'Thermal expansion of natural spinel, ferroan gahnite, magnesio-chromite and synthetic spinel'. Acta. Cryst. A31, 820-822 (1975).

Siripairoje P. 'An investigation into the heat capacities of the superconducting spinels'. PhD Thesis, University of Aston in Birmingham (1978).

Smith P.P.K. 'Note on the space group of spinel materials'. Phil-Mag B38, 99-102 (1978).

Smith T.F., Finlayson T.R. and Shelton R.N. 'Superconductivity and anharmonicity in V_3Si'. J. Less Common Metals 43, 21-32 (1975).

Smith T.F. and White G.K. 'The low temperature thermal expansion and Grüneisen parameters of some tetrahedrally bonded solids'. J. Phys. C: Sol. Stat. Phys. 8, 2031-2042 (1975).

Standley K.J. 'Oxide magnetic materials'. Clarendon Press, Oxford (1972).

Strelkov P.G. and Novikova S.I. 'Thermal expansion coefficients of Aluminium' Prib. Tekh. Eksp. (USSR) 5, 105-110 (1957).

Straumanis M.E. and Woodard C.L. 'Lattice parameters and thermal expansion coefficients of Al, Ag and Mo at low temperature, comparison with dilatometer data'. Acta. Cryst. A27, 549-551 (1971).

Suzuki I. and Kumazawa M. 'Anomalous thermal expansion in spinel $MgAl_2O_4$'. Phys. Chem. Minerals 5 279-284 (1980).

Tabor D. 'Gases, liquids and solids', Penguin Books (1969).

Tachiki M. and Yosida K. 'Antiferromagnetism of Zn-ferrite'. Prog. of Theor. Phys. (Osaka) 17, No.2, 223-240 (1957).

Tanaka M. Tokoro T. and Aiyama Y. 'Jahn-Teller effects on Mossbauer spectra of Fe_{57} in $FeCr_2O_4$ and FeV_2O_4' J. Phys. Soc., Japan, 21, No.2, 262-267 (1966).

Testardi L.R. 'Structural instability, anharmonicity and high temperature superconductivity in A15 structure compounds'. Phys. Rev. B5, 4342-4349 (1972).

Van Uitert L.G. 'Dielectric properties of and conductivity in ferrites'. Proc. IRE 44, 1294-1303 (1956).

Wang C.C., Dougherty F.C., Zanzuchi P.J. and McFarlane S.H. 'Epitaxial growth and properties of GaAs on aluminate spinel'. J. Electrochem. Soc. 121, 571-582 (1974).

Weil L. 'Magnetisme-anomalie de longueur des ferrites'. C.r.hebd. Se'ance. Acad. Sci., Paris, 23, 122-124 (1950).

Westrum E.F. and Grimes D.M. 'Low temperature heat capacity and thermodynamic properties of zinc ferrite'. J. Phys. Chem. Solids 3, 44-49 (1957).

White G.K. 'Thermal expansion of reference materials: copper, silica and silicon'. J. Phys. D.: 6, 2070-2078 (1973).

Williamson D.P. and Grimes N.W. 'An X-ray diffraction investigation of sulphide spinels'. J. Phys. D.: Appl. Phys. 7, 1-6 (1974).

Wilson A.J.C. 'Mathematical theory of X-ray powder diffractometry'. Cleaver-Hume (1963).

Yates B. 'Thermal expansion'. Plenum Press, London, New York (1972).

ACKNOWLEDGEMENTS

I would like to express my gratitude to my supervisor, Dr N W Grimes, for his guidance, patience, encouragement and great help during this work. Without his involvement, I would not be able to persevere and conclude this work.

My thanks to Mrs Grimes and family for their help during the writing of this work.

I would also like to express my gratitude to Professor T Mulvey for his encouragement and help during this work.

My thanks to the technical staff of the Physics Department, in particular to Mr G Cochrane for his assistance during the early part of the experimental work, and to Mr A Reynolds for his assistance during the final part of this work.

My thanks to Mrs C J Davison for typing this thesis.

My gratitude and love to my parents and family who have made it possible for me to come to England to pursue this research and to expand my knowledge.